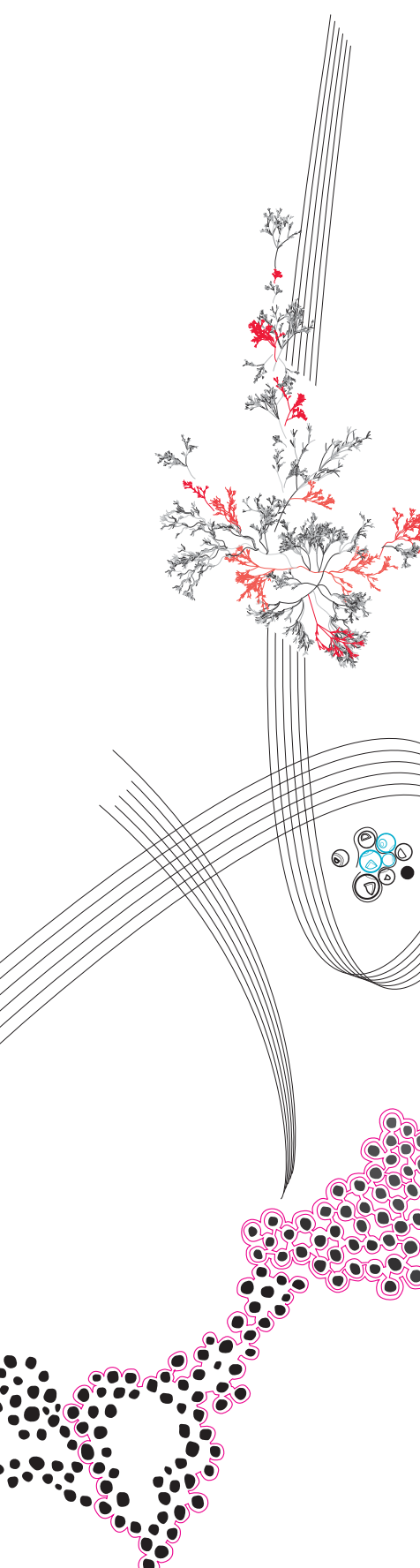MSc Thesis Biomedical Engineering

Design and evaluation of an adjustable step size trajectory generator for the Symbitron exoskeleton with spinal cord injury users

Sterre Triezenberg

Supervisor: Dr. E. H. F. Van Asseldonk
Daily supervisor: A. Vallinas Prieto MSc.
External supervisor: M. K. Maclean PhD.

March, 2024

Department of Biomechanical Engineering
Faculty of Science and Technology
Biomedical Engineering

UNIVERSITY OF TWENTE.

Preface

This research is the thesis for the master Biomedical Engineering at the University of Twente, located in Enschede. The work had been performed at the Department of Biomechanical Engineering, which specializes in integrating various engineering disciplines to analyse and improve human functioning. A focus of the department is committed on balance and exoskeletons. The research on exoskeletons to improve mobility of patients suffering from spinal cord injuries is highly developed.

Abstract

This study presents a controller design and a trajectory generator for the Symbitron Exoskeleton, a lower limb exoskeleton developed for people with a spinal cord injury (SCI). This trajectory generator comprises three different generated trajectories: from a fixed library, with one fixed step length and width; an adjustable library with adjustable step lengths and widths; and a partly adjustable library with a fixed step width and adjustable step lengths. The aim of this study was to develop and experimentally evaluate these libraries, enabling pilots to adjust their step sizes during gait. This is particularly useful for the 'Stones' task of the Cybathlon 2024, an assistive technologies championship. In this task, participants traverse a path of fixed stones without knowing the distances between them and without touching the ground between each stone.

The (partly) adjustable libraries allow the pilot to select from different step sizes, instead of being limited to a single option. This functionality was achieved by computing different step sizes through the trajectory generator and arranging them sequentially according to the pilot's preference. To ensure seamless transitions between these steps, polynomials were incorporated into the controller, effectively smoothing the trajectory. Two experiments were executed involving one healthy male participant. In the first experiment, the pilot was instructed to walk in the lab while making steps of different step sizes. During the second experiment, targets were placed on the ground to indicate desired step lengths and widths. The goal was to evaluate the performance of the libraries in terms of accuracy, precision, task load, and time. Findings from the experiments indicated that fixed and adjustable libraries outperformed the partly adjustable library in terms of accuracy, precision, task load and time. The results of the first experiment were precise but lacked accuracy, particularly in step width performance. In the second experiment, the accuracy, mean error < 5 cm, and precision, standard deviation < 5 cm, were met for step width using the fixed and adjustable libraries. The precision requirement was also met for the step length of those libraries, however, the accuracy requirement only for some of the step lengths. The partly adjustable library exhibited the highest task load, while the fixed library had the lowest. Furthermore, both the fixed and adjustable libraries met the time requirements.

Recommendations for improving the exoskeleton include enhancing joint angle tracking, torque regulation, and expanding the range of available sizes. Future experiments with SCI patients could further validate the performance of the different libraries. Using the (partly) adjustable libraries, the pilot was able to choose between different step sizes, which was not possible before. With this implementation, pilots can now select from different step sizes, enhancing the functionality and usability of the Symbitron exoskeleton for individuals with a SCI.

Contents

1 Introduction

1.1 Clinical picture

A spinal cord injury (SCI) is damage to the spinal cord which can lead to paralysis. It is estimated that, globally, between 250.000 and 500.000 people suffer from SCIs each year. The prevalence in 2020 was 1.298 cases per one million individuals, with numbers continuing to rise [1]. The location and severity of the SCI are important factors for the impact of the injury [2]. The location of the injury can be anywhere along the spinal cord. More body functions will be lost when the location of the injury is more superior. A SCI is referred to as paraplegia when the legs, trunk and pelvic organs are affected. While tetraplegia involves the arms and hands in addition to these areas. The severity of the injury is determined by the completeness of the damage. Patients experiencing an incomplete SCI retain some sensory and/or motor function below the lesion, while an complete SCI results in the loss of all sensory and motor functions.

The impact of SCIs on patients' lives is tremendous. These injuries not only affect patients' ability to walk but also have social, mental, and emotional consequences. Those factors have such a big impact that 37 percent of the people with a SCI suffer from depression as well [3]. This is substantially higher compared to the number of the whole population suffering from depression, which is 3.8 percent [4]. To improve their mobility and quality of life, wearable exoskeletons have been developed. These technical devices, attached to the body, provide support or assistance in physical activities, enabling SCI patients to achieve a level of walking that can allow them to participate more comprehensively in their communities [5]. Nowadays, the acquisition of exoskeletons is too expensive for the personal-use market. The cheapest available model, the ReWalk, is priced at 70.000 dollars [6]. Consequently, exoskeletons are predominantly utilized in experimental settings to advance exoskeleton technologies and in rehabilitation applications. Research has demonstrated the effectiveness of exoskeletons in the rehabilitation of patients with an incomplete SCI. Training the musculoskeletal system using a wearable exoskeleton is crucial for patient's health, preventing cardiovascular disease, weight gain, and other negative outcomes [7].

1.2 Cybathlon

Wearable exoskeletons have significant added value for people suffering from an SCI, and research is ongoing to improve the quality of walking using these devices. One example of a platform promoting the development of assistive technologies is the Cybathlon, which is a championship competition focused on technologies that enhance human performance [8]. The aim of this competition is to encourage technological advancements which can improve the quality of life of people with disabilities. The first edition of this competition was held in 2016 [8]. The upcoming Cybathlon in 2024 has eight disciplines; arm prosthesis, assistance robot, vision assistance, brain-computer interface, exoskeleton, functional electrical stimulation bike, leg prosthesis, and wheelchair race [9]. This edition of the event includes tasks with varying terrains made up of both moving and stationary obstacles which make them way harder to execute. Because of these variations, pre-programmed paths are not sufficient, since the devices need to be able to react to their environment and change their path during the movement. This pushes researchers and engineers to improve their assistive devices.

This study focuses on the exoskeleton race, where the pilot must be capable of completing ten tasks. In the second version of the Cybathlon, held in 2020, the following tasks were included; 'sit and stand', 'slalom', 'rough terrain', 'stairs', 'tilted path', and 'ramp and door'. The winning team, Angel Robotics 1, successfully completed the entire set of tasks within 3 min and 47 s [10].
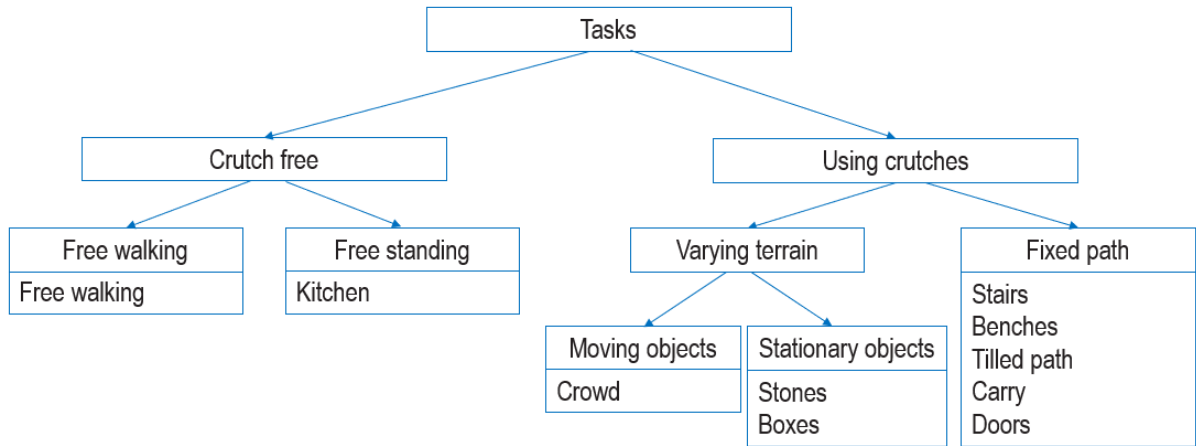
FIGURE 1: Tasks for the Cybathlon 2024 categorized. They are arranged from the hardest (left) to the easiest (right) tasks.

Figure 1 shows all tasks for the upcoming Cybathlon categorized. For tasks falling within the 'crutch free' category, the exoskeleton must maintain balance without relying on crutches. Within the category 'Using crutches', a specific sub-category involves a fixed path. The paths for tasks in these categories are all pre-computable. During task execution, the pilot will not need to make decisions, resulting in relatively fast computational times due to a single available choice. This is not feasible for tasks with varying paths, as the pilot and exoskeleton must react to the environment. There will be more potential options, so the state machine of the exoskeleton will be more complex.

The crutch-free walking or standing task, as well as the one involving moving objects with varying paths, are beyond the scope of this study. The exoskeleton used for this study, see section 1.4, is already capable of executing most of the tasks in the 'fixed path' category using its current trajectory generator [11] and controller [12]. Adapting the implemented trajectory generator could potentially address all tasks with a varying path. However, due to time constraints, the focus of this study will be on the stepping stones tasks. Figure 2 shows a CAD model of this task [13]. The pilot has to walk over a series of stepping stones without touching the red surface, the crutches are allowed to tough this surface. The ability of the pilot to accurately place their feet on locations, which are unknown to them beforehand, is being assessed. To complete this task, the pilot must be able to change step sizes during the gait.
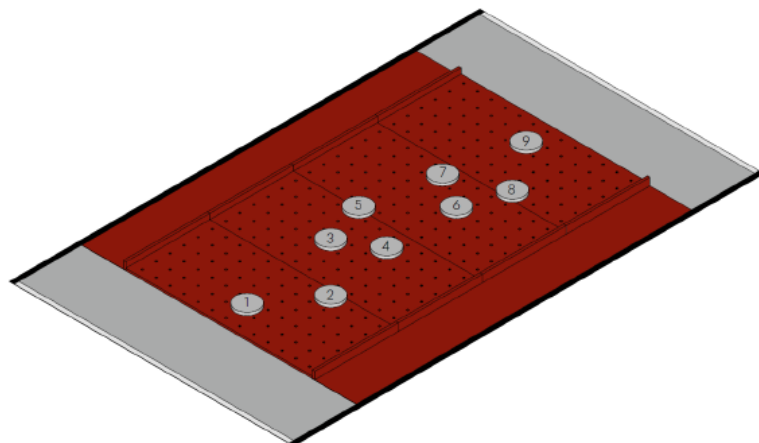

FIGURE 2: CAD model of the stones task for the Cybathlon 2024. The pilot has to walk over a sequence of 9 stones, without stepping on the red surface [13].

1.3 State of the art

Nowadays, most exoskeletons, including the exoskeleton used in this study, are equipped with a real-time controller. However, the reference trajectories are often non-real-time and rely on pre-defined trajectories. Typically, both commercial and research exoskeletons feature four degrees of freedom (DOFs), incorporating active hip and knee joints [14, 15]. These exoskeletons commonly rely on gait profiles derived from healthy human subjects to generate trajectories. Reference trajectories are established based on pre-recorded patterns of healthy individuals, which are subsequently replicated within the exoskeleton [16]. The desired joint trajectories are typically parameterized based on various postures, improving the usability and flexibility of the controller. This approach is used for subjects who lost their voluntary movements partly/completely. However, there are several disadvantageous associated with this approach. Generating sufficient paths requires the recording of numerous walking patterns, which, in turn, demands a relatively large amount of storage. Unfortunately, the availability of such storage can be limited, and it is extremely time consuming to compute all the individual steps. Furthermore, pre-recorded walking patterns lead to partly/completely loss of voluntary movements. The method allows for limited length [17] and speed changes [18]. This occurs because the predefined and fixed patterns, being recorded in advance, may restrict the individual's ability to freely control or modify their movements during the walking process.

Some exoskeletons incorporate an active ankle joint in addition to the standard configuration. Certain systems generate ankle trajectories in task space and employ inverse kinematics to execute these motions [19]. This method has demonstrated flexibility in adjusting step height and length. However, challenges arise when the model encounters singular configurations or when pilot joint limits restrict motion. Alternatively, when integrating an active ankle joint, another approach involves replicating the gait patterns of healthy individuals [19]. This methods adapts healthy gait patterns to modify high-level gait tasks, sharing similar limitations with trajectory generators used for four DOF exoskeletons.
Moreover, some exoskeletons feature an additional active joint for hip ab-/adduction, thereby expanding the DOFs in the frontal plane. These systems also utilize gait pattern generators based on healthy users to enhance flexibility [12]. However, due to the increased complexity resulting from multiple degrees of freedom across different planes, manual adaption of these patterns becomes complex and challenging. Moreover, this process is often time-consuming, with adaptations typically represented in form of polynomials and splines.

Model-based trajectory generation is another often used method. It calculates the desired joint positions and torques directly, considering the zero moment point criterion, gravity compensation, and providing additional instructed support [20]. The zero moment criterion is a specific point on the interface between the ground and the robot at which the net dynamic and static external forces and moments are in balance. This can be done real-time or non-real-time. However, due to the computational complexity of solving dynamic equations, optimization and approximations, this is mostly done non-real-time. The model-based method is employed to assist individuals with muscular weakness, aiding them in mobility and daily activities. It requires various sensors and a high accuracy of the exoskeleton's performance, recognizing dynamic and kinematic variables. Implementing this method becomes hazardous when uncertainties exist regarding the accuracy of the sensors. Running multiple simulations with slightly different input parameters is necessary to find the optimal trajectory, which is why this process is not conducted in real-time.

The approaches used for humanoid robots [1] are also sometimes used in exoskeletons. The Wandercraft exoskeleton [22] adopts the hybrid zero dynamics approach [23], one of several approaches in this field. This approach focuses on generating dynamic gaits that ensure stability by carefully coordinating both the continuous dynamics of the system (e.g. walking) and discrete events (e.g. foot-ground contact). This approach allows for more natural and human-like movement patterns while maintaining stability and flexible motions in the exoskeleton. Notably, this method stands out for its effectiveness in generat-

---

[1]**Humanoid robots** are robots designed to resemble and mimic human characteristics, typically in their appearance, movement, or behavior. These robots often feature a bipedal structure with arms, legs, and a head, allowing them to navigate and interact with their environment in ways similar to humans [21].

ing trajectories for exoskeletons capable of crutch-free walking, relying on precise knowledge of both the pilot's and the exoskeleton's dynamic parameters. Most exoskeletons depend on crutches, which generally makes the requirements for approaches such as hybrid zero dynamics too demanding for such systems.

A commonly employed approach involves the development of simple models that incorporate boundary condition for joint trajectories at specific waypoints, followed by the fitting of a mathematical curve to these trajectories [24]. This is a relatively straightforward method to apply with great adaptability to the user and the gait. However, this approach does not allow changing walking parameters during gait, making it impossible to avoid obstacles or navigate in difficult situations. IHMC Robotics also utilized waypoints in its approach [25, 26].

IHMC Robotics secured second place in the Cybathlon 2016 with the Mina v2 exoskeleton [26] and fourth place in the Cybathlon 2020 with the Quix exoskeleton [25]. Both exoskeletons shared the same trajectory generation design. The swing leg trajectory was computed using four Cartesian positions and velocity waypoints. The start and end point were waypoints, and two intermediate waypoints were included. The swing trajectory is parameterized by step length, swing duration, initial foot position, waypoint height, and waypoint fraction. An online gradient descent optimization is used to minimize the intermediate waypoint velocities by varying the segment durations, creating the trajectories. The stones task was included in the Cybathlon 2016, and IHMC Robotics was one of the two teams who completed this task [26]. However, in contrast to the stones task in the Cybathlon 2024, the sequence of stones was known in the 2016 edition. During the Cybathlon 2020, the stones task was replaced by the a rough terrain obstacle, including unavoidable wooden logs [25]. The principle of the tasks remains the same, using visual input to determine the appropriate placement of the feet while avoiding specific locations.

IHMC Robotics attributes their success in the Cybathlon 2016 to the high flexibility in the walking patterns due to Cartesian waypoints for the swing foot [26]. This trajectory design allows for easy adjustments of step lengths and times. Consequently, the Quix' trajectory design is well-suited for the aforementioned tasks, as well as other tasks of the Cybathlon. However, it is crucial to note that in the Cybathlon 2016, all paths were predefined and known. In the Cybathlon 2024, where the sequence of the stones is unknown, this method would not be effective, as the pilot must be able to change their step length and width during gait to execute this task. The inclusion of an interface to switch between trajectories is essential.

Because of the varying terrain of the Cybathlon 2024 'Stones' task, having a real-time trajectory generator would be advantageous, allowing for updating the walking parameters at any time, and enabling the pilot to select the next step during gait [27]. Kazemi and Ozgoli propose a real-time minimum jerk walking pattern generator for the Exoped exoskeleton [24]. In this method, the walking parameters (step length, maximum foot clearance, stride time) can be changed without discontinuity in the second derivative of the trajectories during the stride. The joint position feedback controller is designed to ensure the system's output satisfies the boundary conditions of the trajectories. A minimum jerk cost function is implemented to convert the trajectory planning problem into an optimal control problem, including changeable final states. It is important to note that, since the walking parameters are computed in real-time in this method, the stability of the robot it not fully taken into account, potentially leading to safety risks (e.g. falling). Additionally, real-time trajectory generation is currently not frequently used due to the long computational time and the considerable amount of computational power needed.

1.4 Symbitron exoskeleton

1.4.1 Hardware and controller

The University of Twente is set to participate in the Cybathlon 2024 with the Symbitron exoskeleton, designed for pilots suffering from Paraplegia [2]. Two crutches are demanded for support while walking in this exoskeleton, with mechanical buttons on one crutch serving as the control interface. One button initiates weight shifts and steps, while another button handles the weight shift and stepping phase of the closing step [12]. The exoskeleton comprises a total of ten DOFs, including eight active and two passive [11]. Figure 3 gives an schematic overview, including all joints and actuators. Active DOFs control the hip ab- and adduction, hip flexion and extension, knee flexion and extension, and ankle dorsi- and plantarflexion. Notably, each leg possesses four active joints, resulting in a cumulative count of eight active DOFs for the entire exoskeleton across both legs. Meanwhile, the hip internal and external rotation, as well as the ankle inversion and eversion, are passive joints, and can be locked if demanded [12].

The Symbitron exoskeleton has a two-part control structure consisting of low-level and high-level control [12]. The low-level control involves individual joint control, where the desired torque for each joint's output shaft is generated. To accomplish this, the required motor torque is determined by a disturbance observer. Using this method, the system disturbances are estimated by employing the inverse of the nominal plant model, and a high-bandwidth low-pass filter. The bandwidth of this low-pass filter has the purpose to maximize disturbance estimation within the system's robustness constraints [28]. The high-level control, which will be the focus of this study, regulates the exoskeleton's behavior by determining the amount of torque to be exerted on each joint. A speed-dependent reference joint trajectory generator algorithm is implemented and controls the hip and knee joint trajectories by providing reference trajectories for continuous walking [29]. The current trajectory generator used in the Symbitron exoskeleton is the optimization-based trajectory generator developed and implemented by Rampeltshammer et al [11].
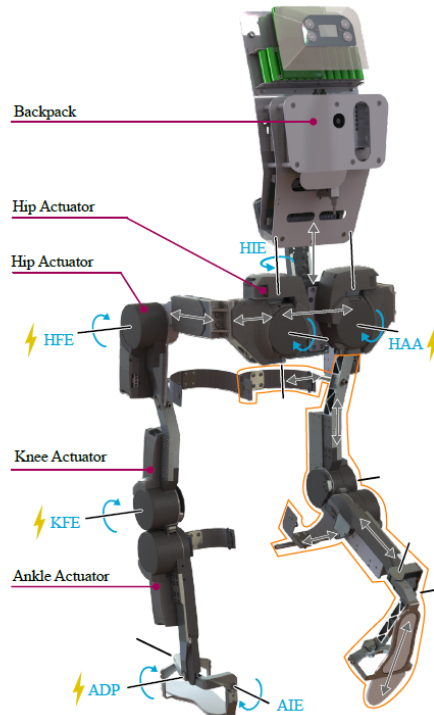

FIGURE 3: CAD-model of the Symbitron exoskeleton. Illustrating all active, hip ab-/adduction (HAA), hip flexion/extension (HFE), knee flexion/extension (KFE) and ankle dorsi-/plantarflexion (ADP), and passive, hip internal and external rotation (HIE) and ankle inversion/eversion (AIE) joints [12].

1.4.2 Trajectory generator

The output of the trajectory generator constitutes a stance trajectory, which allows for flexible position shifting by the pilot when in double stance, and swing trajectory, which generates an optimized trajectory when in swing phase. The reference trajectories are obtained non-real-time using a technique similar to that implemented in the Mina v2 and Quix exoskeletons, outlined in Section 1.3. This technique involves deriving boundary conditions of the joint trajectories and fitting them to a polynomial curve [11, 24].

When the exoskeleton is in double support phase, it performs a weight shift in both the sagittal and frontal planes. The objective of this motion is to transfer the center of mass (COM) from the trailing leg to the leading leg, facilitating a smooth transition between steps. This weight transfer is followed by the stepping phase, during which the exoskeleton moves the leg through the step cycle. The currently used trajectory generator computes joint trajectories in the form of time polynomials. A fifth-order time polynomial was used to represent the desired motion, ensuring continuity and meeting boundary conditions. These polynomials were concatenated to achieve the desired motion, with specific phases like weight shift and stepping consisting of multiple fifth-order polynomials sequenced to maintain motion continuity. Section 2 will delve deeper into the characteristics and applications of these polynomials.

This trajectory generator computes a path that has an opening step, an intermediate step and a closing step. The initial pilot parameters, representing the configurations of the exoskeleton in the initial state (a stationary parallel stance), are used as the starting values for the optimization. These values are utilized to determine the polynomial coefficients for the weight shift of the opening step. The optimized polynomials of the weight shift for that step are employed to obtain the polynomials for the stepping trajectories of that opening step. The output of one optimization is a set of polynomial parameters, the output polynomial defines the beginning of the next one, ensuring a connection between the motions. The same principle applies to the intermediate and the closing steps, where the optimized output values of the weight shift for each respective step are taken to obtain the corresponding polynomial coefficients for the stepping trajectories. For the weight shift of the intermediate step, the output values of the stepping motion from the opening step are employed. For the weight shift of the closing step, the output values of the stepping motion from the intermediate step are taken. Figure 4 describes the required inputs to obtain the polynomials. Since all steps have the same step length, height, and width, a closing step can also be executed after an opening step, and an intermediate step after an intermediate step. After completing the closing step, the pilot should stand in parallel stance. However, the joint angles might not perfectly match the desired neutral position. Hence, the exoskeleton requires homing to ensure it returns to the correct alignment after the stepping phase of the closing step. This is done by implementing a first-order polynomial between the end values and the desired begin positions.
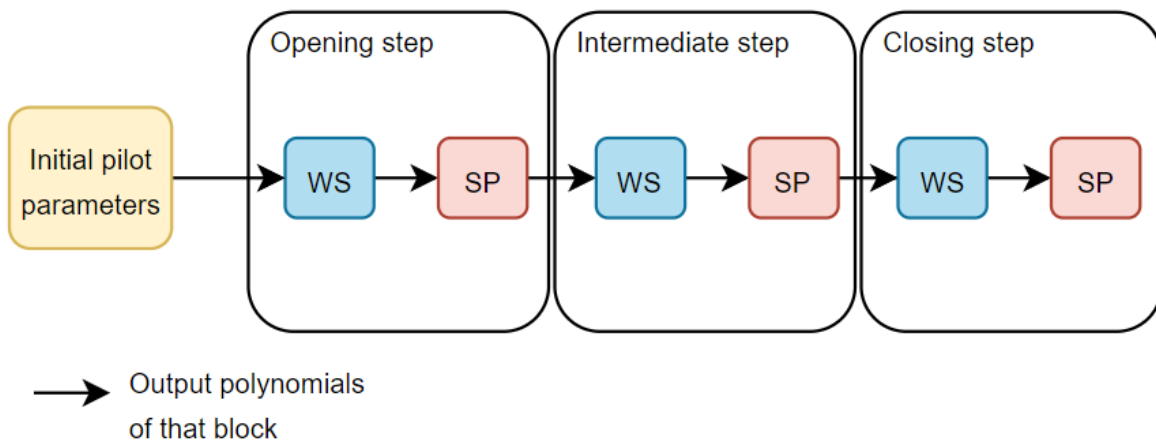

FIGURE 4: Diagram describing the required input polynomials to obtain the output polynomials for the weight shifts (WS) and stepping phases (SP) of all three step types.

The gait cycle consists of distinct phases; the single support phase and the double support phase, each characterized by nonlinear constraints, which constitute the high-level gait tasks. These tasks involve initiating movement, coordinating weight transfer, ensuring foot clearance, adjusting step height, and reaching the step target. By including nonlinear constraints and a parametrization of joint trajectories, the joint angle trajectories can be optimized to achieve C^2 continuity and fulfill high-level gait tasks, respectively [11]. C^2 continuity is achieved in a polynomial when its acceleration exhibits smoothness over time. One of the requirements of the used trajectory generator is that the joint trajectories must be C^2 continuous, ensuring comfort for the user. This C^2 continuity is a constraint that completely defines three parameters per polynomial. The other polynomial coefficients are obtained through the constrained minimization of the cost function (Equation 1) [11].

$$J = \int_0^T || \dddot{q} ||^2_{W_1} + ||\ddot{q}||^2_{W_2} + ||\dot{x}||^2_{W_3} + ||\theta - \theta_d||^2_{W_4} dt \tag{1}$$

After the optimization parameters are obtained, comfortable motions are ensured by this cost function that minimizes joint jerk ($\dddot{q}$), joint acceleration ($\ddot{q}$) and COM velocity ($\dot{x}$) of the trajectory, as well as keeping the trunk orientation as steady as can be [11]. The latter is achieved by determining the error between the desired lean angle (θ_d) and the actual lean angle (θ).

A major advantage of the currently used trajectory generator is its flexibility compared to similar systems, especially the ones using predefined gait trajectories [16]. This trajectory generator easily adapts to various gait patterns by customizing individual high-level gait tasks, so fast adjustments of parameters (e.g. step height) is possible, as well as adapting to the sizes of the pilot [11]. The pilot for the Cybathlon 2024 is not yet determined, allowing the possibility of selecting a pilot at a later stage. The shift of the COM in the double support phase is very well-controlled by the high-level controller using this trajectory generator due to the highly constrained motions. However, the used implementation of the trajectory generator generates a single opening step, an intermediate step, and a closing step. Consequently, this design limits the pilots' control over their walking path, as they cannot adjust the step size during gait, except for initiating the steps and stopping the gait. The implementation of multiple step sizes has not been investigated for this trajectory generator thus far.

1.5 Goal of the study

This study aims to develop and experimentally evaluate a trajectory generator and controller for the Symbitron exoskeleton, allowing pilots to adjust their step sizes during gait for tasks such as the Cybathlon 2024 'Stones' task.

The goal of this study is to design a trajectory generator and controller with specific outcome metrics for a downscaled version of the 'Stones' task: step size accuracy and precision less than 5 cm, a task completion time under 2 min, and a transition time, the duration needed to select and operate a single step, under 20 s. The currently used trajectory generator and controller in the Symbitron exoskeleton serve as a foundation for developing a new trajectory generator to achieve these goals. Three different types of trajectories were incorporated, called libraries: a fixed, adjustable, and partly adjustable. The fixed library computes one step length and one step width. The adjustable library develops steps with different step lengths and widths. The partly adjustable library generates steps with a fixed step width and varying step lengths.

Specifically, the study poses the research question: 'Which of the three libraries from the trajectory generator and controller achieves the best accuracy, precision and fastest transition and task completion time when completing a downscaled version of the Cybathlon 2024 'Stones' task?' The three different libraries will be tested by performing experiments, further details about the experiments will be elaborated in the next section.

This paper will discuss the rationale behind the obtained requirements and modification made to the trajectory generator and high-level controller (Section 2.1), the experimental setup and evaluation process (Section 2.2), the results obtained (Section 3), and the conclusions drawn from the findings, as well as the limitation and utility of the study (Section 4).

2 Methodology

This section represents a trajectory generator and high-level controller with three distinct libraries, including an adjusted high-level controller. The requirements for the design are outlined, followed by a detailed explanation of the three libraries and their implementation. Those designs were experimentally evaluated and compared with each other, by executing two experiments.

Throughout the entire study, the following coordinate system conventions were used; the x-axis corresponds to the walking direction, the z-axis represents the right-lateral direction, and the y-axis denotes the direction opposite to gravity.

2.1 Adjusted trajectory generator and high-level controller

The trajectory generator, including three libraries, and controller were developed based on specified requirements. The design decisions are detailed and clarified in this section.

2.1.1 Step sizes

For the Cybathlon 2024 'Stones' task, two distinct options for step length (0.525 and 0.252 m) and step width (0.525 and 0.375 m) are prescribed. These step dimensions significantly differ from the typical step sizes, being both longer and wider (typical step length = 0.35 m and step width = 0.47 m).

The given step dimensions pose a challenge for the algorithm responsible for computing step sizes. Specifically, aiming for such large and small target step lengths and widths leads to the violation of both linear and nonlinear constraints within the exoskeleton's design. From the linear constraints, the hip ab-/adduction joint angles are violated. Additionally, nonlinear constraints associated with step height of the foot, target ankle, target foot, and target COM are also breached. These constraint violations have consequences for the trajectories. The trajectory generator, responsible for obtaining them, fails to reach an optimal solution. A proper kinematic behavior cannot be reached without adhering to both linear and nonlinear constraints. To address the constraint violations, a solution was investigated: multiplying the virtual lengths of the exoskeleton in the trajectory generator by a factor of 1.3. While a pragmatic approach, it becomes clear that increasing segment lengths is necessary to achieve the required step lengths and widths. This adjustment does lead to an optimal solution without violating any of the linear or nonlinear constraints. This means the problem is too constrained for all nonlinear and linear constraints which are implemented in the trajectory generator. Violating these constraints prevents task satisfaction and results in compromised kinematic behavior of the exoskeleton. This results in trajectories which are not continuous. When this occurs, the controller of the exoskeleton detects the breaks in the trajectories and cannot process them, therefore generating an error. Table 1 shows the segment lengths of the exoskeleton for reference.

Table 1: Segment lengths of the exoskeleton

Upper leg:	0.430 m
Lower leg:	0.400 m
Foot height:	0.125 m
Ankle to toe distance:	0.230 m
Heel to ankle distance:	0.058 m

Given the unfeasibility of executing step sizes of both large and small magnitudes from a kinematic standpoint, this study employs more moderate step sizes (step length = 0.3 and 0.35 m, step width = 0.5 and 0.45 m). It is crucial that all combinations of step length and width remain feasible. Thus avoiding extremes in size, neither too large nor too small, is necessary. This approach ensures accurate and precise assessment of the libraries without encountering issues arising from excessively large or small step sizes, which could introduce errors or deviations. Consequently, the two experiments, to be discussed later in this study, utilized these moderate step sizes.

2.1.2 Requirements

This section specifies the requirements for the trajectory generator. The diameter of the stones used in the Cybathlon is 25 cm. To ensure the pilot's stability and prevent the risk of falling off the stone, the midpoint of the pilot's foot should remain within a 15 cm diameter. This allowance provides a 5 cm safety margin on all sides. In this scenario, the pilot positions at least two-thirds of their foot onto the stone. Considering the foot's total length of 28.8 cm (sum of 23 cm and 5.8 cm, see Table 1) and accounting for the measurement from the foot's midpoint, half of the foot is always located on the stone. Incorporating the 5 cm safety margin, the foot is always on the stone with at least 19.4 cm, which exceeds two-thirds of the total foot length. This minimizes the chance that the pilot will fall off the stone. Figure 5 illustrates the stepping stone including the maximum error area. To accomplish this, the mean error with respect to the stepping stone center location ($e_{mean} = \frac{\Sigma_{n=1}^{N}(step\ size\ error)}{N}$, with N = the amount of steps taken during the trials) should be less than 5 cm. Additionally, the standard deviation (STD) should not exceed 5 cm.
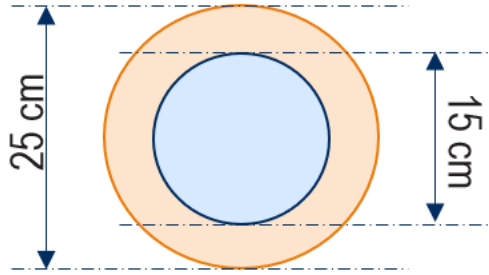

FIGURE 5: Stepping stones and the maximum error area. The orange and blue circles together describe the diameter of the stepping stone. The blue circle depicts the area where the pilot is allowed to position the midpoint of their feet.

In the Cybathlon 2020, the winning time for a similar task was 32 s [10]. However, the 'Stones' task at the Cybathlon 2024 is more challenging due to the varying terrain. This will likely result in a decreased task completion speed. Therefore, the time for completing the task was set at 2 min. Each individual step, including the selection of the desired step size, should not take too long either; therefore, the requirement of the transition time of one step is set to less than 20 s. It is important to consider that task completion is more crucial compared to the task's speed, as failure to complete the task would eliminate the participant from that segment of the competition. Consequently, the accuracy and precision requirements are considerably more stringent compared to the time. Table 2 summarizes these requirements.

TABLE 2: Requirements of the design

Accuracy: mean error	<5 cm
Precision: STD	<5 cm
Time of task:	<2 min
Transition time of one step:	<20 s

2.1.3 Polynomial trajectory generation

Like mentioned in the introduction, the trajectory is constructed of several polynomials. To be specific, a fifth-order time polynomial. Equation 2 describes a simple fifth-order polynomial. The rationale behind this order will be explained later in this section.

$$q(t) = a_0 + a_1 x + a_2 x^2 + a_3 x^3 + a_4 x^4 + a_5 x^5 \tag{2}$$

The six parameters $(a_0, a_1, a_2, a_3, a_4, a_5)$ were computed such that the boundary conditions are satisfied. These boundary conditions define the initial and final positions (q_i, q_f), velocities $(\dot{q}_i, \dot{q}_f)$ and accelerations $(\ddot{q}_i, \ddot{q}_f)$ of the polynomial. The desired motion is achieved by concatenating several of these polynomials one after the other. To achieve continuity in the motion, the starting point of a polynomial is defined by the ending point of the previous motion. The weight shift and stepping phase consists of two and four fifth-order polynomials, respectively, put behind each other to achieve the desired motion.

During the double support phase, the constraints ensure that both feet remain on the ground and that the COM is shifted from the trailing leg to the leading leg. During single support phase, the constraint is to maintain the COM over the leading leg. In addition to the nonlinear constraints, linear constraints are also implemented to ensure that the trajectories adhere to the kinematic limitations imposed by either the exoskeleton or the pilot. These constraints account for upper and lower limits in the joint angles, velocities and accelerations.

Equation 3 describes the joint trajectories for each joint d [11]. The trajectories are a combination of N polynomials of the Kth order. The indication function δ_p determines whether polynomial p is active.

$$q_d(t) = \Sigma_{p=1}^{N}(\delta_p(t)\Sigma_{k=0}^{K}(^d a_{k,p} t^k)) = \Sigma_{p=1}^{N}(\delta_p(t)^d a_p^T T), \tag{3}$$

where t is time, T is vectorized time, $^d a_{k,p}$ are the polynomial coefficients, and $^d a_p^T$ are the vectorized coefficients. $^d a_p^T$ represents a combination of the coefficients in $^d a_{k,p}$ with time instances T up to the Kth order. K is set to 5 to have enough unconstrained parameters and achieve C^2 continuity. N = 2 in the double support phase and N = 4 in the single support phase. Those are selected in order to minimize the number of unknowns [11]. Equation 4 describes how the polynomial coefficients are computed.

$$^d A = \begin{bmatrix} ^d a_0 \\ . \\ . \\ . \\ ^d a_n \end{bmatrix} = {}^A P_Q \cdot Q_0 + {}^A P_a \cdot {}^d \hat{A}, \tag{4}$$

with Q_0 as the initial and $^d \hat{A}$ as optimized parameters. C^2 continuity is achieved by multiplying the projection matrices $^A P_Q$ and $^A P_A$ with those parameters.

2.1.4 Libraries

Three different libraries were implemented in the trajectory generator and the controller of the exoskeleton. The first library, referred to as fixed library, is based on the original trajectory generator developed by Rampeltshammer et al [11]. This library computes steps with uniform lengths and widths for all steps, with predefined values of L = 0.35 m, W = 0.47 m for this study. This width remains the original implemented width in the trajectory generator without any additional width. The selection of this step length is based on its compatibility with the chosen width. This combination had been found to produce a smooth and effective gait pattern. The second and third library, referred to as the adjustable library and partly adjustable libraries, respectively, are modified versions of this original trajectory generator. These modifications enable the generation of steps with varying lengths and widths during the gait. The adjustable library has adjustable step lengths and widths. Conversely, the partly adjustable library has an adjustable step length and a fixed step width. In this library, the pilot must manually change their heading, direction which the pilot is facing, to guide the foot to the correct target. This is done by placing the crutches, and adjusting the upper body posture. The step sizes were computed non real-time in the trajectory generator. However, the controller is determining which step will be performed real-time, as well as computing the polynomials, making this a partly real-time exoskeleton.

As previously stated, the fixed library remains the currently used trajectory generator unchanged. The principles of generating steps in the (partly) adjustable libraries are similar to that of the fixed library, described in section 1.4.2.

For the experiments, two different step lengths and widths were utilized, resulting in four possible step sizes. This results in four opening steps, four intermediate steps, and one closing step. The closing step, designed to transition the pilot to a parallel stance, remains constant regardless of the step length or width. Each of those steps were created to allow the pilot to transition from each opening step to every intermediate step and closing step. Additionally, from every intermediate step, another intermediate step and the closing step were obtained. In total, there are 44 weight shifts and 44 stepping phases, ensuring a possible transition between all required steps. Figure 6 provides a visual representation of how this total is computed. During operation, the pilot only needs to select from the four available step sizes. The controller will subsequently determine the right choice among the 44 possible weight shifts and stepping phases. This determination considers the previous step size, the next step size, and the type of step (i.e. initial, intermediate, or closing).
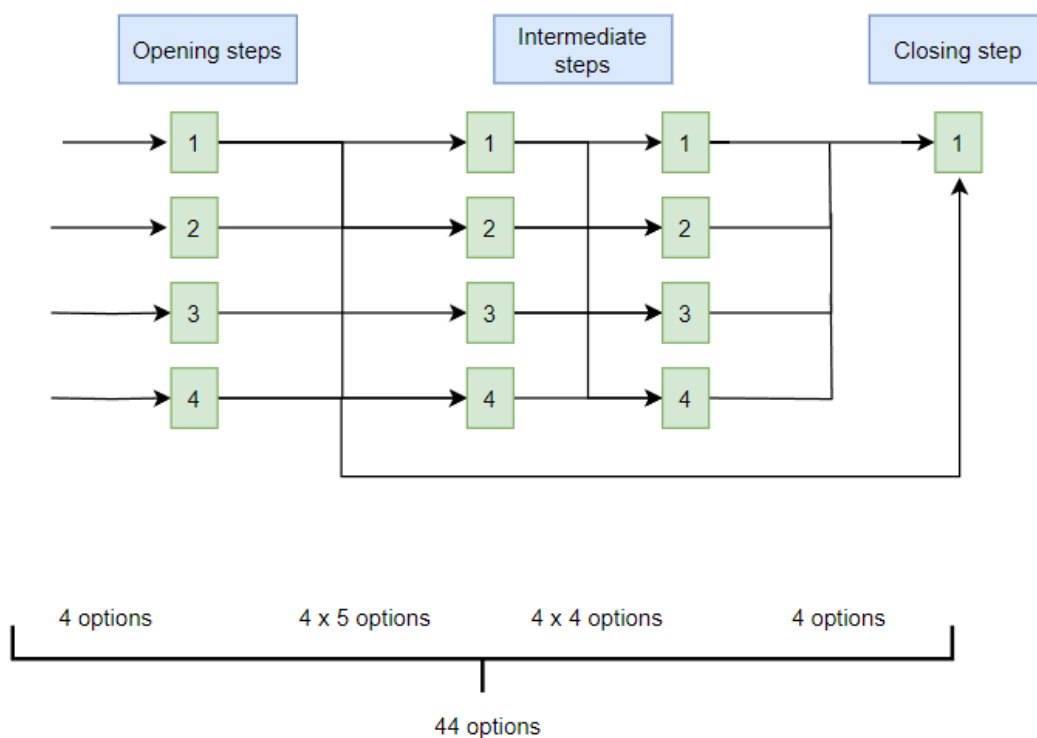

FIGURE 6: Overview of the computation of the amount of step options for the (partly) adjustable libraries.

As previously mentioned, the adjustable library maintains step lengths and widths that correspond to those used in the experiments. Alternatively, the partly adjustable library utilizes a fixed step width ($SW = 0.47$). To compute the step lengths in this library, the diagonal between the desired step length and width was calculated. Once this diagonal was determined, the fixed step width was used to compute the step lengths, using the Pythagorean theorem, as shown in Equation 5. This was possible since the diagonal is the same for both steps. A schematic overview of this calculation is depicted in Figure 7. Table 3 displays the step lengths and width for the different libraries.

$$SL_{new} = \sqrt{(diag)^2 - (SW_{fixed})^2}, \ with$$
$$diag = \sqrt{(SL_{original})^2 + (SW_{original})^2}$$

(5)

Step length computation of partly adjustable library

(A)   (B)
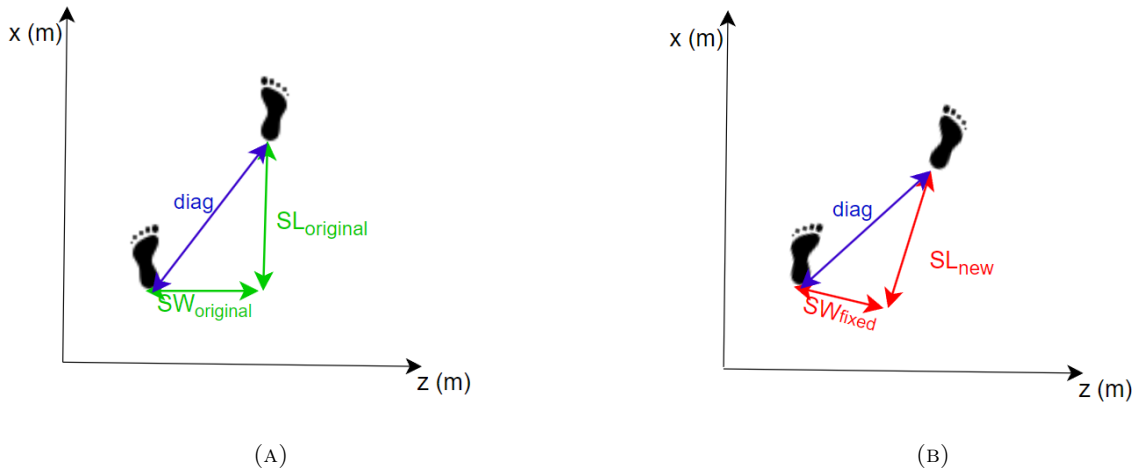
FIGURE 7: Schematic top view of the pilot taking a step. The diagonal between the original step length ($SL_{original}$) and width ($SW_{original}$) is computed to generate the step length (SL_{new}) for the partly adjustable library, considering the fixed step width (SW_{fixed}) of 0.47 m. $SL_{original}$ and $SW_{original}$ are perpendicular, as well as SL_{new} and SW_{fixed}. The diagonal in both figures is the same length, which proves that this computation is valid.

	Fixed	Adjustable	Partly adjustable
Step size 1 (m)	SL = 0.35 SW= 0.47	SL = 0.35 SW = 0.5	SL = 0.39 SW = 0.47
Step size 2 (m)	-	SL = 0.35 SW = 0.45	SL = 0.32 SW = 0.47
Step size 3 (m)	-	SL = 0.3 SW = 0.5	SL = 0.35 SW = 0.47
Step size 4 (m)	-	SL = 0.3 SW = 0.45	SL = 0.27 SW = 0.47

TABLE 3: Step lengths (SL) and widths (SW) for the different libraries corresponding to the four step size numbers.

In the original design, all steps maintained the same duration. However, given the variations in step dimensions, it is reasonable to adjust the duration to ensure consistent velocities across all steps. The duration was calculated using Equation 6. The virtual velocity was set to 0.32 m/s, being set as default in the exoskeleton's controller. This 'virtual velocity' is not a true velocity since the velocity is not constant throughout the entire step. Instead, it serves as a guideline to determine the correct duration so that this duration across all step sizes is evenly distributed.

$$Duration = \frac{step\,length}{virtual\,velocity} \tag{6}$$

Figure 8 presents the outcomes of the trajectory generator for the different libraries. The figure illustrates that the actual step length aligns with the desired step length across all libraries. However, the desired step width only corresponds to the actual step width in the adjustable library. For the other two libraries, it deviates by 0.02 m. Similarly, the desired step height deviates by 0.02 - 0.03 m across all libraries. It is worth noting that the validation of this study does not include the integration of step height, making it less critical for the analysis.

Evaluation of the computed walking parameters
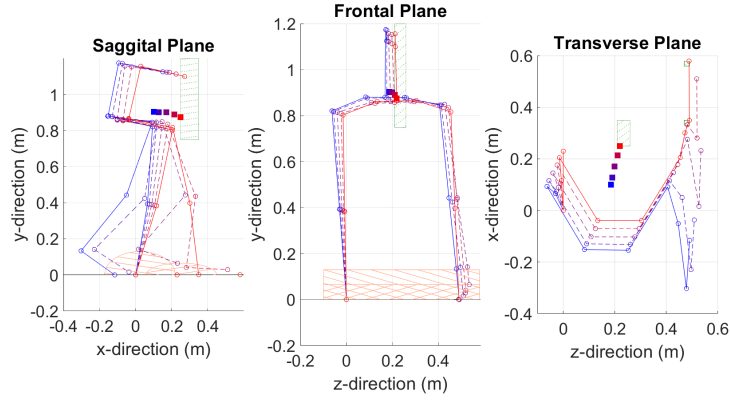
(A) Fixed library
$SL_{des} = 0.35$ m, $SW_{des} = 0.47$ m, and $SH_{des} = 0.13$ m,
$SL_{act} = 0.35$ m, $SW_{act} = 0.49$ m, and $SH_{act} = 0.16$ m.
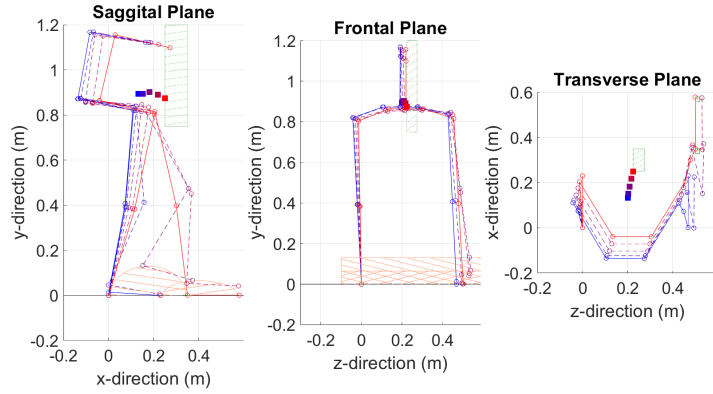
(B) Adjustable library
$SL_{des} = 0.35$ m, $SW_{des} = 0.5$ m, and $SH_{des} = 0.13$ m,
$SL_{act} = 0.35$ m, $SW_{act} = 0.5$ m, and $SH_{act} = 0.15$ m.
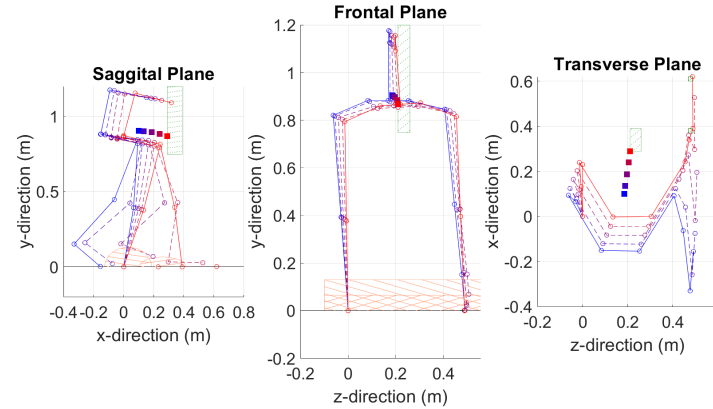
(C) Partly adjustable library
$SL_{des} = 0.39$ m, $SW_{des} = 0.47$ m, and $SH_{des} = 0.13$ m,
$SL_{act} = 0.39$ m, $SW_{act} = 0.49$ m, and $SH_{act} = 0.15$ m.

FIGURE 8: Simulated outcome parameters of the trajectory generator with the different libraries including the desired step length (SL_{des}), step width (SW_{des}), step height(SH_{des}), and the actual step length (SL_{act}), step width (SW_{act}), step height(SH_{act}).

2.1.5 Continuous and smooth signal

Figure 9 shows the hip ab-/adduction joint trajectory with the acquired parameters for the adjustable library. It demonstrates gaps in between the stepping phase of the previous step, and the weight shift of the next step.

Hip ab-/adduction joint angle during four simulated steps using the adjustable library
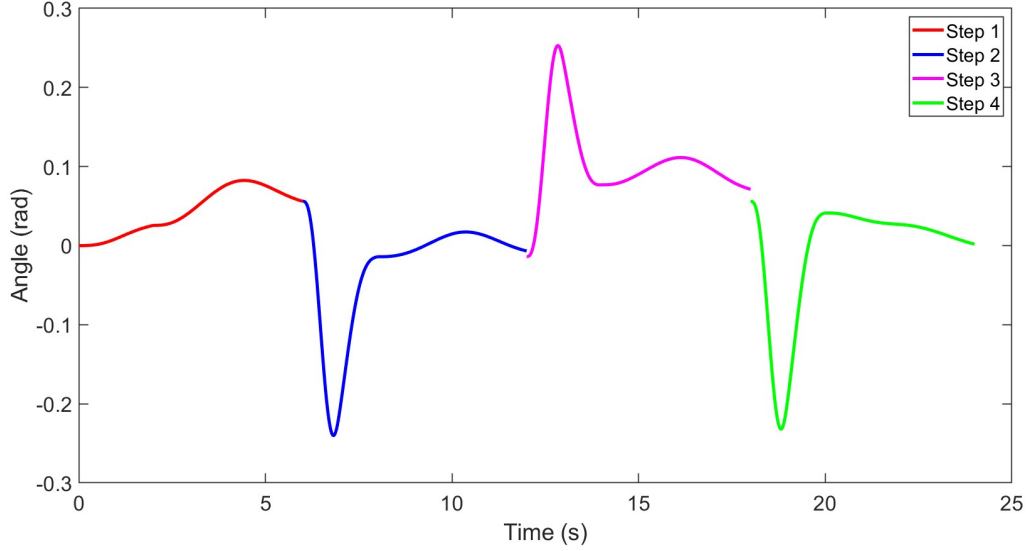

FIGURE 9: Simulation of the trajectories with the acquired parameters of the adjustable library. The red graph illustrates the weight shift and stepping phase during the opening step with the right leg, while the blue graph represents the corresponding phases of an intermediate step with the left leg. Similarly, the purple and green graphs represent subsequent steps in the sequence.

When executing consecutive steps, it is essential for the initial position of each step to match the final position of the previous step. Different step sizes can lead to different final positions, creating a discontinuity where the initial position of one step does not align with the final position of the previous step. To resolve this issue, a proposed solution is necessary to ensure continuity in the sequence of steps.

From Figure 9, it is evident that there is no gap between the opening step (step 1) and the first intermediate step (step 2). The weight shifts of the intermediate steps were computed using the output polynomials of the stepping phase of the opening steps. This approach ensures a smooth connection between all opening steps and subsequent ones.
When transitioning from an intermediate step (step 2) to another intermediate step (step 3), a gap is observed. The polynomials for step 3 are derived from the output polynomials of step 2. However, when the step before the previous step is different, the polynomials may not be exactly the same. This inconsistency appears due to optimization, where the output values are not always identical. Additionally, while the location of the end effector may be the same, this does not imply the outcome of all joint configurations is the same as well, this could lead to a incontinuous signal. Due to this complexity, just considering the current en previous step size is insufficient. Resulting in a computation of $(4 \cdot 4 =)$ 16 step sizes being inadequate.

To ensure smooth transitions between steps, it would be theoretically possible to compute all possible steps from every possible preceding step. However, this approach would results in an excessive number of steps, calculated as $(4 \cdot 4^8 \cdot 1 = 262.144)$. This number is obtained by multiplying the number of options at each step throughout the sequence of ten steps: one openings step, eight intermediate steps, and one closing step. The number of options grows by a factor of 4 at each step, since there are four options for

each next step. This is highly inefficient and would require substantial computational resources.

Therefore, an alternative solution has been implemented to address this issue. To fill the gaps between the steps, a fifth-order polynomial was computed by the controller in real-time. This polynomial acts as a flexible connector, smoothly interpolating between known points in the trajectory to ensure continuity and accuracy. The order of this polynomial ensures that the trajectory remains C^2 continuous, maintaining the same smoothness as the rest of the trajectory. A gap is detected when the difference in angle between the previous time step and the current time step exceeds the threshold value, which is set at 0.01 radians. When the gap is smaller than this threshold, the controller is capable of compensating for the gap itself by linearly interpolating the path between the points.

The polynomial is generated using the angle (q), angular velocity($\dot{q}$) and angular acceleration($\ddot{q}$) at the end of the polynomial before the gap (P_x) as starting condition. The q, $\dot{q}$ and $\ddot{q}$ of the beginning of the polynomial after the gap (P_{x+1}) are used as end conditions. The parameter values for the polynomials are obtained using equation 7. This computation needs to be performed separately for each joint.

$$parameters = F^{-1} \cdot Q \tag{7}$$

using,

$$F = \begin{bmatrix} 1 & 0 & 0 & 0 & 0 & 0 \\ 1 & T & T^2 & T^3 & T^4 & T^5 \\ 0 & 1 & 0 & 0 & 0 & 0 \\ 0 & 1 & 2T & 3T^2 & 4T^3 & 5T^4 \\ 0 & 0 & 2 & 0 & 0 & 0 \\ 0 & 0 & 2 & 6T & 12T^2 & 20T^3 \end{bmatrix} \tag{8}$$

$$Q = \begin{bmatrix} q_{endPx} \\ q_{startPx+1} \\ \dot{q}_{endPx} \\ \dot{q}_{startPx+1} \\ \ddot{q}_{endPx} \\ \ddot{q}_{startPx+1} \end{bmatrix} \tag{9}$$

T is the time interval for one polynomial, ranging from 0 to 1. This value for T is taken for the general computation of the polynomials. Afterwards, this polynomial, together with the weight shift and stepping phase polynomials, will be scaled to their actual duration, velocities, and acceleration. Equations 10, 11, and 12 are used for that, respectively.

$$q = T_{mat} \cdot paramameters \tag{10}$$

$$\dot{q} = T_{mat} \cdot R_{mat} \cdot paramameters \tag{11}$$

$$\ddot{q} = T_{mat} \cdot R_{mat} \cdot R_{mat} \cdot paramameters \tag{12}$$

The function T_{mat}, as defined in Equation 13, ensures the correct allocation of parameters to each joint, while also scaling them appropriately based on given time instances. On the other hand, using the function R_{mat}, described in Equation 16, the derivatives of joint angles were calculated, thereby facilitating the computation of joint velocities and accelerations.

$$T_{mat} = \text{eye}(n) \otimes rate^{(0:5)}, \tag{13}$$

with n being the amount of joints, which is 11 in this case, was inserted in an identity matrix. The rate represents the time instant within the current polynomial, Equation 14. The rate transitions from exponent 0 to 5 since it is a fifth-order polynomial like described in Sections 1.4.2 and 2.1.3.

$$rate = mod(time\ location, 1 + eps) \tag{14}$$

This method uses Equation 15 to compute the time location, which represents the time instant within the current weight shift or stepping phase. This information is crucial for determining the active polynomial within that part of the step.

$$time\ location = \frac{time}{duration} \cdot n \tag{15}$$

The variable time represents the time instant within the gait cycle of the exoskeleton, ranging from 0 to the duration of each weight shift (including gap filling) or stepping phase. n represents the number of polynomials: two for the weight shift, three for the weight shift including gap filling, and four for the stepping phase. Therefore, the gap filling is an additional polynomial implemented before the weight shift.

R_{mat} is calculated using Equation 16.

$$R_{mat} = dt \cdot diff\ matrix, \tag{16}$$

with dt and the differentiation matrix given by Equations 17 and 18, respectively.

$$dt = \frac{1}{duration} \cdot n \tag{17}$$

$$diff\ matrix = \text{eye}(n) \otimes diag(1:5, 1) \tag{18}$$

n is the amount of joints, 11, inserted in an identity matrix. On the main diagonal of this 6 times 6 matrix, the vector 1:5 is taken, with one diagonal above the main diagonal filled with zeros.

Once the polynomial to fill the gap was determined, it was integrated into the signal. The gap filling was incorporated into the intermediate step between the stepping phase of the previous step and the weight shift of the upcoming step, provided that the gap between the polynomials is at least 0.01 radians. Figure 10 illustrates the trajectory of the hip ab-/ adduction joint including the polynomials that filled the gaps. The gap filling process takes place within the high-level controller and was implemented for the (partly) adjustable libraries.

Hip ab-/ adduction joint angle during four simulated steps using the adjustable library including gap filling
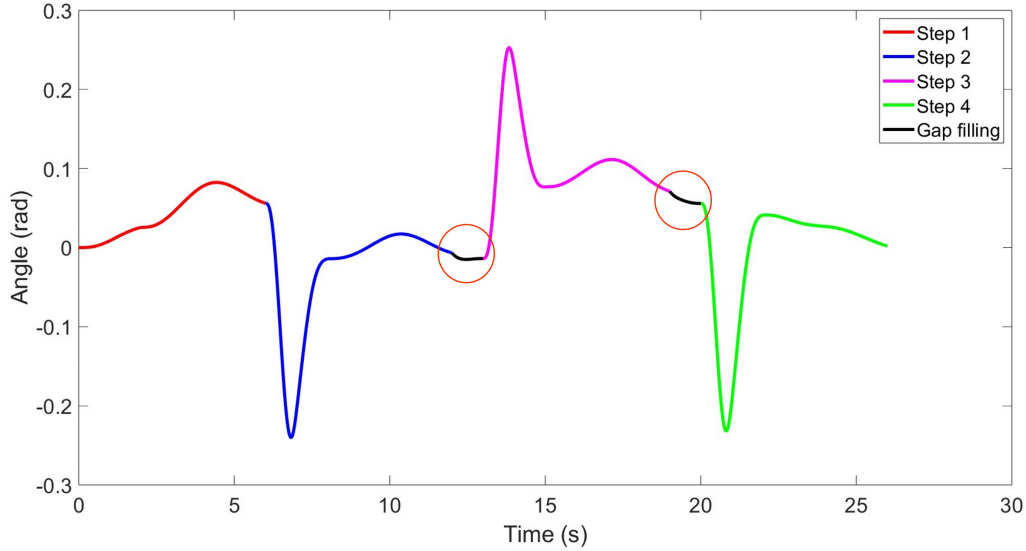

FIGURE 10: Simulation of the trajectories with the acquired parameters of the adjustable library including polynomials to fill the gaps. The red graph illustrates the weight shift and stepping phase during the opening step with the right leg, while the blue graph represents the corresponding phases of an intermediate step with the left leg. Similarly, the purple and green graphs represent subsequent steps in the sequence. The black lines illustrate the gap fillings.

2.1.6 High-level controller

Adjustments were made to the high-level controller to enable the selection of the correct path and execution of trajectories effectively. These modification are applied to the currently utilized high-level controller. The primary modifications in this controller involve the state machine and parameter implementation. The state machine will be discussed first.

Several adjustments were made to the state machine. Firstly, pilots now have the capability to change the starting leg, allowing them to choose which leg to start with. This feature has been implemented across all libraries. Secondly, a new modification allows pilots to adjust the step size of the next step. This adjustment can occur at two distinct time instances: during parallel stance, and prior to a weight shift. It is not possible to change the step size after the weight shift. The weight shift facilitates the transfer of the COM from the trailing leg to the leading leg, preparing the exoskeleton for the subsequent stepping phase. Any attempt to modify the step size between the weight shift and stepping phase would result in mismatched polynomials, leading to disconnecting trajectories. For a more detailed exposition of the implementation, please refer to Appendix 6.1.

Within the parameter implementation, modifications were made in both the parameters selection and angle computations. In the (partly) adjustable libraries, a total of 44 distinct steps had been implemented for both left and right legs. The determination of the correct polynomial for the chosen step involves considering the active leg, the previous step size, the step type, and the desired step size. Appendix 6.1 provides an elaborated overview of how the step sizes can be chosen and executed. Furthermore, a graphical user interface (GUI) was created to facilitate straightforward interaction with the system. Figure 11 demonstrates this GUI, providing pilots with clear visibility of the selected and facilitating ease of adjustment. Additionally, awareness of the gait type and starting leg is essential for the pilot to anticipate upcoming movements. Furthermore, an algorithm detects gaps between step transitions, filled by gap-filling polynomials outlined in Section 2.1.5.
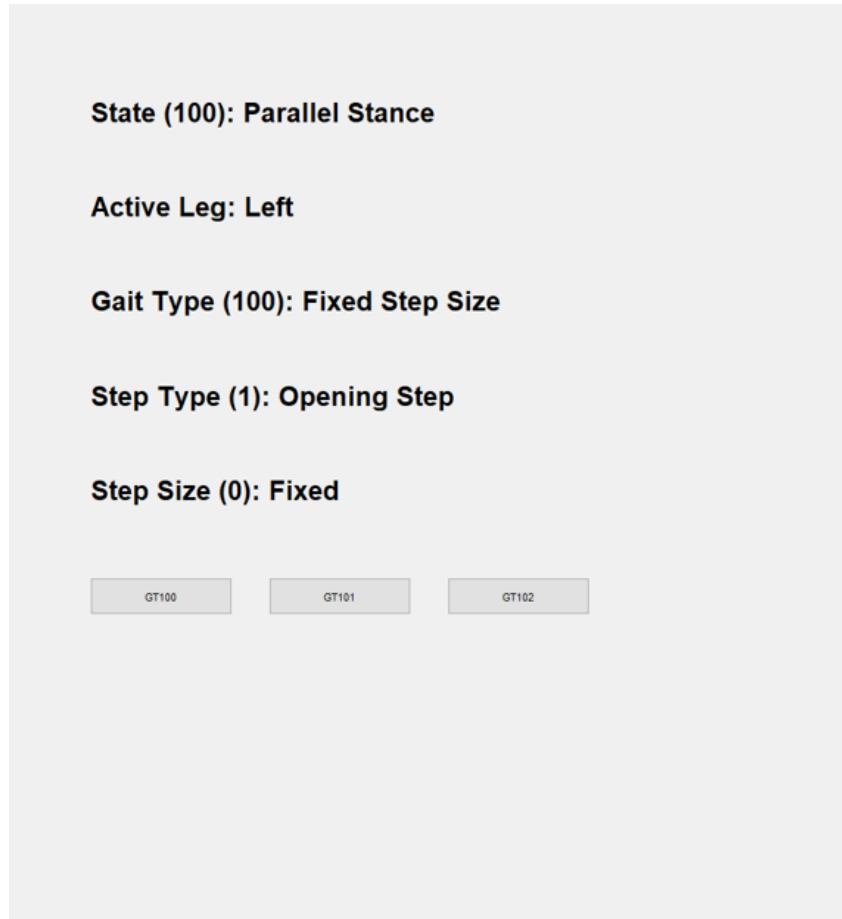
FIGURE 11: Screen shot of the part of the GUI important for the pilot. Showing the step type, step size and active leg, among other things.

2.2 Experimental evaluation

Two experiments were executed to compare the accuracy, precision, task load, task completion time, and transition time of the three different libraries. These experiments are based on the Cybathlon 2024 'Stones' task.

2.2.1 Participants

One healthy pilot (male, age= 28) of good physical condition was included in the study.

2.2.2 Experimental equipment

For this study, the Symbitron exoskeleton from the EU Symbitron Project was used [12]. The experiment was performed in the Wearable Robotics lab at the University of Twente. This lab includes a ten camera motion capture system (Qualisys AB, Göteborg, Sweden), and a ZeroG Gait and Balance system [2] (Aretech, Sterling, USA). For this experiment 26 reflective markers were used. The sample frequency of the marker data recordings was 128 Hz. The joint positions, velocities and torques were recorded at 1000 Hz in the exoskeleton.

---

[2] The **ZeroG Gait and Balance system** is a robotic tool designed to provide dynamic body weight support during rehabilitation therapy. It utilizes overhead tracks and a harness to enable patients to walk safely [30]

2.2.3 Protocol

The markers were placed by the researcher using the Plug-In-Gait lower-limb model and additional markers on C7 [3], sternum, the shoulders, and one additional marker on each foot, shown in Figure 12. These markers were used for accurate and precise capture of movements of those specific points for gait analysis. The exoskeleton and Qualisys system were turned on, and the Qualisys system was calibrated. The ZeroG system was attached to the exoskeleton to prevent the pilot from falling. During the first experiment, the pilot was instructed to walk ten predetermined steps in the Symbitron exoskeleton in three different trials, conducted for all three libraries. This process was repeated three times. After each trial, the pilot used the ZeroG system to turn around. Given the absence of visual input, no targets displayed on the ground, the pilot relied solely on the movements of the exoskeleton. The objective of this experiment was to assess the accuracy, and precision of the libraries while the visual information for proper foot placement guidance was missing.

In the second experiment, the pilot was instructed to traverse a predefined sequence of targets, as depicted in Figure 13a. The different colors represent three sequences of steps that the pilot must walk through. These varied sequences allow for more step combinations, while keeping short trials. Figure 13b shows one of the trials including step lengths and width between the targets. The pilot was instructed to position the midpoint of the foot on the center of the cross. The pilot walked again in the exoskeleton using all proposed libraries three times in each trial. After completing each trial, the pilot was turned by the ZeroG system and brought back to the beginning of the path. The goal of this experiment was to evaluate the performance of the libraries when the pilot is aware of the target. The complete protocol for these experiments can be found in Appendix 6.2.

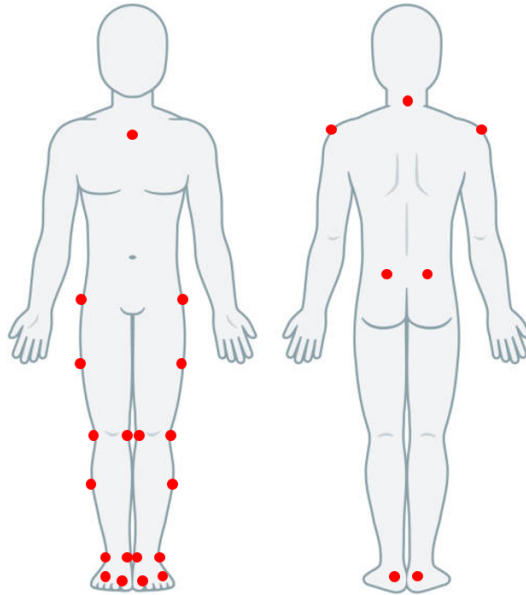FIGURE 12: Human body diagram including the required markers according to the Plug-In-Gait lower-limb model and additional markers on C7, sternum, the shoulders, and one additional marker on each foot.

---

[3]**C7** refers to the seventh cervical vertebra, which is the lowest bone in the neck (cervical spine) region. It plays a crucial role in providing structural support and facilitating movement of the head and neck [31].

Experimental setup

(A)   (B)
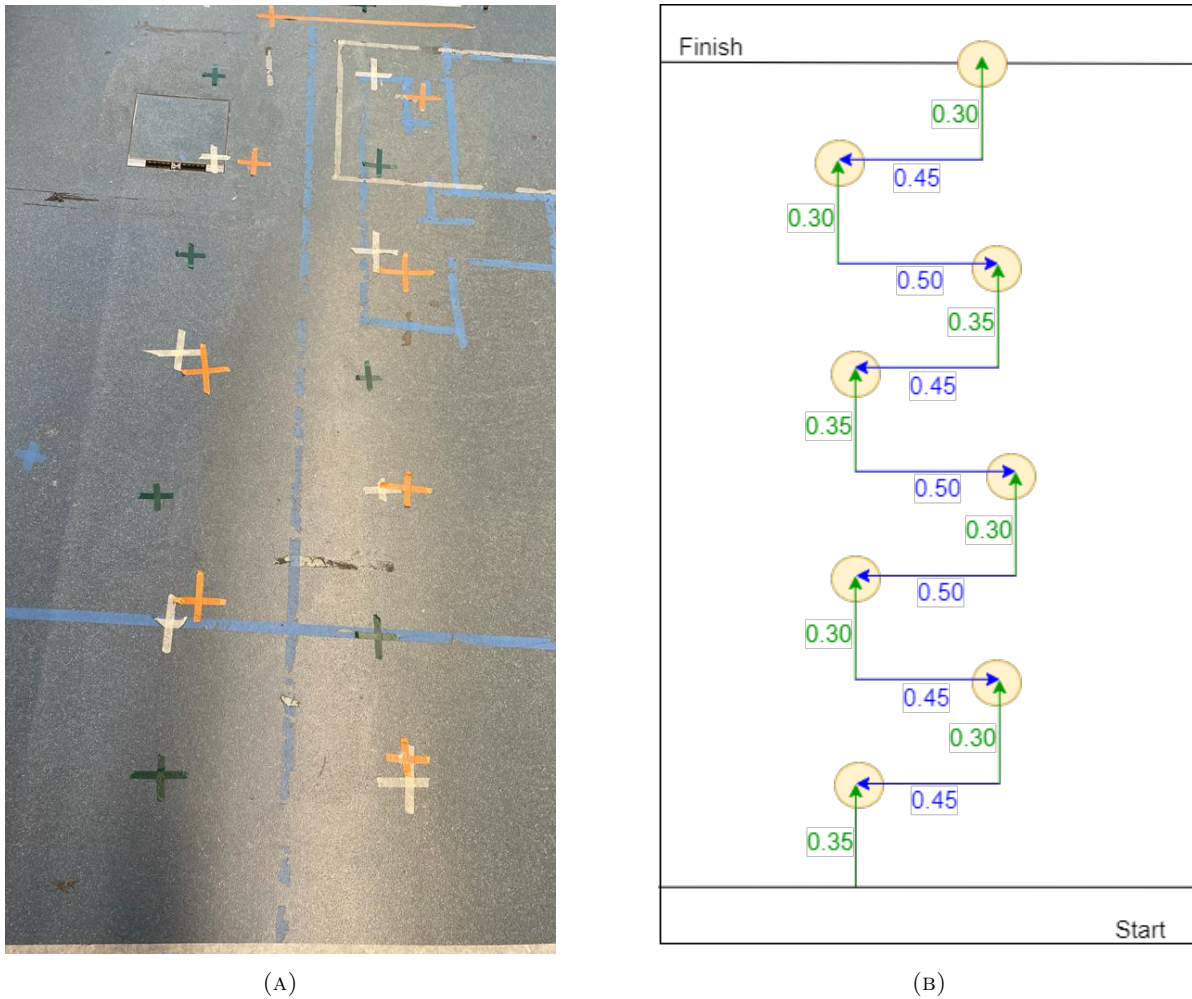
FIGURE 13: Experimental setup A) utilized during the experiment, with three colored tapes indicating the sequences of target steps. B) A scaled schematic overview, featuring yellow circles representing the error areas of the targets, blue arrows denoting step width distances, and green arrows indicating step length distances. This illustration corresponds to the green trial.

Lastly, the participant was asked to complete the NASA task load index (NASA-TLX), Appendix 6.6. This questionnaire was employed to assess the demands and difficulty levels of the libraries during the experiment. Every part was assessed on a scale of 21 gradations indicating whether the load is high, medium, or low. The higher the score, the more intense the work load.

2.2.4 Data analysis

The output of the three libraries and high-level controller were validated with the data from a single pilot. The Qualisys data was used to compute the lengths and widths of each step, with the Qualisys interface determining the moments when the the pilot was in double stance. The three different libraries were validated through assessing their performance based on the accuracy and precision of the steps. Alongside computation of the task completion time and the transition time of each step. Furthermore, the output of the exoskeleton's controller was examined to ensure alignment with the desired output. The markers on the upper body were used to determine whether there were variations in the posture and movements of the pilot across the different libraries and experiments. This validation process provided insights into the functionality and effectiveness of the trajectory generator and controller, including the

three libraries, providing information on whether the output data was aligned with the desired data.

The Qualisys data was imported into MATLAB (R2023a) for analysis. The step length and width for each step were computed. In Experiment 1, markers were placed on the lateral side of the ankle to determine these step length and width errors. These markers were reliably detected by the Qualisys cameras, which was advantageous for accuracy. However, the kinematic model of the exoskeleton considers the middle of the foot in the frontal plane as the end effector. Unfortunately, the marker on the medial side of the ankle was not visible throughout the whole trial. Consequently, it was impossible to compute the mean between the medial and lateral ankle markers to determine the precise step width. To address this issue, adjustments were made based on the marker's known lateral position, which is 5 cm away from the midline. To account for the 5 cm on each foot, 10 cm were subtracted from the width calculation. This discrepancy does not impact the calculation of step length as long as the markers are in the same position on the sagittal plane.

The walking direction for this experiment was not along either the global x-axis or the z-axis but a rotation around the y-axis was included, the position of the markers placed on the lateral sides of the hips (see Figure 12 for reference) was used to determine this rotation (Figure 14). Equation 19 shows the equation how the angle between the hips was calculated, using the markers placed on both hips.

$$\theta_{hip} = tan^{-1}(\frac{\Delta X}{\Delta Z})$$

(19)

The step length and width were determined using Equation 20 and 21, respectively. The length and width were determined when the pilot was in double stance.

$$length = \frac{\Delta X}{cos(\theta_{hip})}$$

(20)

$$width = \frac{\Delta Z}{cos(\theta_{hip})}$$

(21)
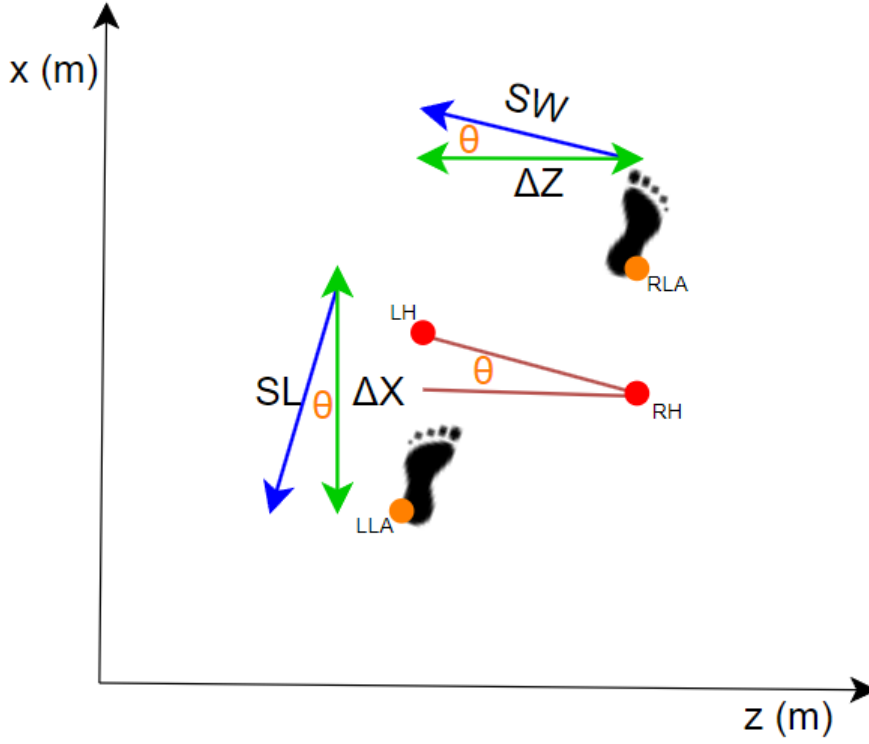
FIGURE 14: Schematic top view of the pilot taking a step. This figure is used to calculate the step length (SL) and width (SW). The red dots represent the left hip marker (LH) and right hip marker (RH). The green arrows represent the difference in x- and z-coordinates of the left lateral ankle marker (LLA) and the right lateral ankle marker (RLA).

To determine the accuracy and precision of the step length, the mean error (Equation 22) and STD (Equation 23) were calculated, respectively. The same procedure to compute the mean error and STD was performed for the step width as well.

$$Mean\ error = \frac{\sum(SL_i - SL_{des})}{total\ numbers\ of\ steps} \tag{22}$$

SL_i represents the actual step lengths, while SL_{ref} denotes the desired step length. The desired step length and widths can be found in Table 3.

$$STD = \sqrt{\frac{\sum(SL_i - SL_{mean})^2}{number\ of\ steps}}, \tag{23}$$

with SL_{mean} being the corresponding mean of the lengths, which was computed with Equation 24.

$$SL_{mean} = \frac{\sum SL_i}{total\ numbers\ of\ steps} \tag{24}$$

24

For Experiment 2, the target steps were positioned to align with the global x- and z-axis for the step length and width, respectively. This arrangement ensured that the step width corresponded to the difference in z-coordinates of the ankle markers, while the step length corresponded to the difference in x-coordinates of the same ankle markers. Δx and Δz were utilized to calculate the step length and width, respectively.

When computing the step length and width using the same methodology as in Experiment 1, cumulative errors may arise due to potential influence of errors from previous steps on subsequent ones. To address this issue, the x- and z-position of the targets were computed using Qualisys, and the position of the placed feet was then subtracted from these target locations. Step length and width errors were determined using markers placed on the medial and lateral sides of the both ankles. The actual foot position was computed by taking the mean of the z-coordinates of the medial and lateral markers. The step width error (e_{width}) was calculated using Equation 25.

$$e_{width} = z_{target} - \frac{(z_{medial} + z_{lateral})}{2} \tag{25}$$

The step length error (e_{length}) was calculated similarly using the x-coordinates, as shown in Equation 26. Additionally, 5 cm was added to account for the marker positions, considering they are not located at the midpoint of the foot.

$$e_{length} = x_{target} - \frac{(x_{medial} + x_{lateral})}{2} + 0.05 \tag{26}$$

The mean error of the width for Experiment 2 was calculated using Equation 27.

$$Mean\ error = \frac{\sum e_{width}}{numbers\ of\ steps} \tag{27}$$

Additionally, the STD of the width for this experiment was computed using Equation 28. The same equations were used to calculate the mean error and STD of the step length.

$$STD = \sqrt{\frac{\sum e_{width}^2}{number\ of\ steps}}, \tag{28}$$

For Experiment 2, the task completion time and the transition time of each step were determined. This is relevant as Experiment 2 serves as a representative simulation of the 'Stones' task of the Cybathlon. The task completion time was calculated as the mean duration across all trials for the three different libraries. One trial is when walking one of the sequences of 9 steps. This time is from the moment the researcher instructed the pilot to start and provided the first step size, until the pilot reached the finish line. This method also accounted for the time needed to choose the initial step size and starting leg. The transition time of each step was computed as the mean duration from the moment the pilot landed in double stance until they returned to double stance again. This ensured that the time taken for step selection was appropriately factored into the time of the subsequent step.

The exoskeleton's controller data was used to compute the tracking errors. The desired joint angles ($q_{desired}$) and measured joint angles ($q_{measured}$) were used to compute the joint tracking error (e_{joint}), using Equation 29. The torque tracking error (e_τ) was computed with the desired torque ($\tau_{desired}$) and the measured torque ($\tau_{measured}$), using Equation 30. The measures are useful to determine the performance of the controller's regulation of the joint angles and torques.

$$e_{joint} = q_{measured} - q_{desired} \tag{29}$$

$$e_\tau = \tau_{measured} - \tau_{desired} \tag{30}$$

The saturation error ($e_{saturation}$) was determined to check whether the desired torques exceeds the torque boundaries. Equation 31 described how this was calculated using the desired torque ($\tau_{desired}$) and the limited torque ($\tau_{limited}$). This is necessary to see if, and how often the desired torques exceed the torque limits.

$$e_{saturation} = \tau_{limited} - \tau_{desired} \tag{31}$$

The posture of the upper body could also have an influence on the positioning of the feet. To investigate this, the roll, pitch and yaw were calculated through the locations of the sternum, and the left and right shoulder markers. These angles correspond respectively to the lateral tilting, forward or backward inclination, and rotational adjustments of the pilot's body on the vertical axis. Figure 15 gives a overview of these rotations.
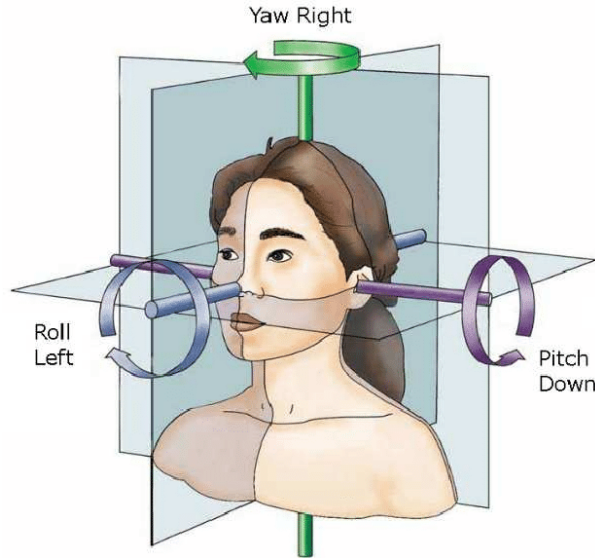
FIGURE 15: Schematic overview of the roll, pitch and yaw angles [32].

To get these rotation angles, two vectors were computed to determine the displacement from point P_1 (sternum) to point P_2 (right shoulder), and from point P_1 to point P_3 (left shoulder), Equation 33 shows the computation of those vectors.

$$V_1 = P_2 - P_1 \tag{32}$$
$$V_2 = P_3 - P_1 \tag{33}$$

The next step was to compute the vector representing the Z-axis of the body frame, Equation 34, and afterwards normalize this value, Equation 35.

$$Z = V_1 \times V_2 \tag{34}$$

$$Z = \frac{Z}{\|Z\|} \tag{35}$$

The X-axis vector was determined using Equation 36, and normalized using Equation 37.

$$X = \frac{(P_1 + P_2)}{2} + P_3 \tag{36}$$

$$X = \frac{X}{\|X\|} \tag{37}$$

The Y-axis vector was computed using Equation 38. This is already a unit vector since X and Z are also unit vectors.

$$Y = Z \times X \tag{38}$$

The rotation matrix representing the orientation of the body-fixed frame is represented by Equation 39.

$$R = \begin{bmatrix} X_1 & Y_1 & Z_1 \\ X_2 & Y_2 & Z_2 \\ X_3 & Y_3 & Z_3 \end{bmatrix} \tag{39}$$

The roll, pitch and yaw were computed with Equations 40, 41, and 42, respectively. The $atan2$ is employed to calculate the roll and pitch angles. This ensures a comprehensive angle representation regardless of the signs of its arguments.

$$Roll = atan2(-Z_2, Z_3) \tag{40}$$

$$Pitch = asin(Z_1) \tag{41}$$

$$Yaw = atan2(-Y_1, Z_1) \tag{42}$$

Statistical analysis

To evaluate significant differences among the output data of the libraries, a one-way analysis of variance (ANOVA) was performed using the Matlab function anova1 [33]. The resulting F-statistics and p-values were obtained. The F-statistic quantifies the ratio of variance observed among group means to the variance observed within the groups. Meanwhile, the p-value indicates the probability of observing the data (or more extra data) assuming there is no significant difference between the groups.

3 Results

In this section, the validation and comparison of the three libraries were performed.

3.1 Accuracy and precision of steps

Figure 16 provides a visual representation of the errors in step length and width, along with their distributions for various step sizes with the three libraries, obtained in Experiment 1. Each individual data point is depicted in a scatter plot, with step length and width errors plotted along the x-axis and z-axis, respectively. The red cross denotes the position where there is no error in either step length or width, while the red circle represents the area of the maximum error. This circle serves to visually assess whether the pilot successfully reaches the stepping stone. It is important to note that these visual aids are for reference only. Above and right from the scatter plot, distributions of data for step lengths and widths are displayed, including their mean and STD. A black stripe within the distribution indicates zero error, indicating perfect accuracy. The fine lines next to this line display the edges of the red circle, which will be referred to as target boundaries. These figures were generated using the Scatter distribution figure function developed by Eline Zwijgers is used [34]. The dataset adheres to a normal distribution (see Appendix 6.3), and so Gaussian distributions were employed to generate these figures. Details regarding mean error and STD can be found in Table 4.

TABLE 4: The mean error and STD of the absolute step lengths en widths, for the different libraries for Experiment 1. It is presented in the form: mean error ± STD.

		SL= 0.35 SW = 0.47 (fixed) SW= 0.5 (others)	SL= 0.35 SW= 0.45	SL= 0.3 SW= 0.5	SL= 0.3 SW= 0.45
Length (m)	Fixed library	-0.023 ± 0.037			
	Adjustable library	0.044 ± 0.037	0.043 ± 0.041	0.119 ± 0.035	0.096 ± 0.039
	Partly adjustable library	0.053 ± 0.037	0.057 ± 0.051	0.116 ± 0.040	0.111 ± 0.057
Width (m)	Fixed library	-0.173 ± 0.019			
	Adjustable library	-0.193 ± 0.025	-0.113 ± 0.049	-0.201 ± 0.022	-0.153 ± 0.016
	Partly adjustable library	-0.207 ± 0.013	-0.113 ± 0.058	-0.199 ± 0.019	-0.155 ± 0.022

Regarding the step lengths, Figure 16a illustrates that the results of the fixed library (mean error = 0.023 m) fall within the accuracy requirement, which necessitates a mean error of less than 0.05 m. The figure also shows that the peak of the distribution is close to zero, and most data points fall within the target boundaries. The other sub figures show that this is not consistently observed for the (partly) adjustable libraries, contributing to the larger mean errors. While the adjustable library meets accuracy requirements for some step lengths, it fails to do so for others. The partly adjustable library does not meet the step length accuracy requirement for any of the step lengths. The precision requirement (STD must be less than 0.05 m) is met for all step lengths of the fixed and adjustable libraries. However, for the partly fixed library, this does hold for step sizes 2 and 4. This was also observed by the spread evident in the distribution plots.

No significant difference in step lengths was observed between different step sizes of the (partly) adjustable libraries. For the step lengths, the f-statistic was 0.95, and the p-value was 0.33. Those values indicate no significant differences among group means and states that the variance among group means is relatively similar to the variance within groups. This means there is no significant difference between the libraries. The significance difference between the step length and widths of the (partly) adjustable libraries compared to the fixed library cannot be computed due to the smaller amount of data points.

Concerning step width data, it is notable that none of the data points fall within the target boundaries. This is due to the deviant step widths, explaining the significant mean errors in all cases. None of the libraries meet the accuracy requirement for the step width. The STD's of the step widths are generally

smaller than those for step lengths. The precision requirement (STD must be less than 0.05 m) is met for all step widths, except for step size 2 of the partly adjustable library, which is 0.058 m. For the step width, the f-statistic was 0.24, with a p-value of 0.63. These values indicate no significant differences among group means and states that the variance among group means is relatively small compared to the variance within groups. This indicates there is no significant difference between the libraries.

Distribution of the different step sizes of Experiment 1

(A) SL = 350 mm & SW = 470 mm

(B) SL = 350 mm & SW = 500 mm

(C) SL = 350 mm & SW = 450 mm

(D) SL = 300 mm & SW = 500 mm

(E) SL = 300 mm & SW = 450 mm
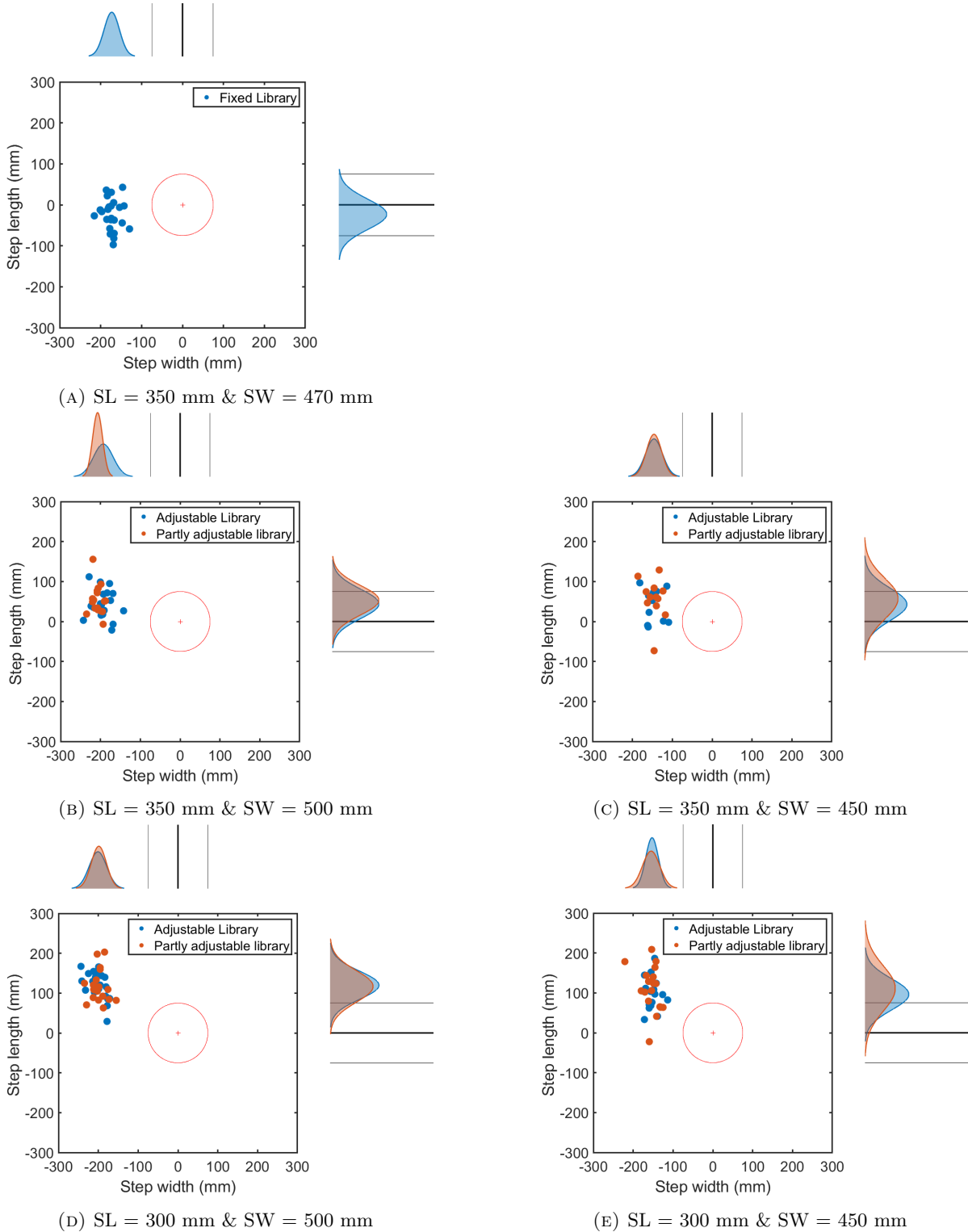
FIGURE 16: Scatter plot showing the data points and the distributions on the x- and z-axis for A) Fixed library, B) (Partly) adjustable library with step size 1, C) (Partly) adjustable library with step size 2, D) (Partly) adjustable library with step size 3, and E) (Partly) adjustable library with step size 4. The black strip indicates the point in the distribution where there is zero error, while the thin black lines show the target boundaries. The red circle highlights the area of maximum error, and the red cross indicates the position where there is no error in either step length or width.

31

Figure 17 shows the distribution and scatter plots of the step length and width errors for Experiment 2. The data follows a normal distribution, as calculated similarly to the approach detailed in Appendix 6.3). Consequently, a Gaussian distribution is employed to generate these figures. The values for the mean error and STD can be found in Table 5.

TABLE 5: The mean error and STD of the absolute step lengths en widths, for the different gait types for Experiment 2. It is presented in the form: mean error $\pm$ STD.

		SL= 0.35 SW= 0.5	SL= 0.35 SW= 0.45	SL= 0.3 SW= 0.5	SL= 0.3 SW= 0.45
Length (m)	Fixed library	-0.055 $\pm$ 0.035	-0.039 $\pm$ 0.019	-0.035 $\pm$ 0.031	-0.037 $\pm$ 0.049
	Adjustable library	-0.055 $\pm$ 0.029	-0.043 $\pm$ 0.017	-0.046 $\pm$ 0.030	-0.052 $\pm$ 0.030
	Partly adjustable library	-0.083 $\pm$ 0.028	-0.084 $\pm$ 0.017	-0.072 $\pm$ 0.022	-0.070 $\pm$ 0.024
Width (m)	Fixed library	-0.030 $\pm$ 0.035	-0.005 $\pm$ 0.023	0.016 $\pm$ 0.033	0.002 $\pm$ 0.027
	Adjustable library	-0.010 $\pm$ 0.020	-0.001 $\pm$ 0.028	0.017 $\pm$ 0.041	0.023 $\pm$ 0.035
	Partly adjustable library	-0.035 $\pm$ 0.047	-0.005 $\pm$ 0.042	0.003 $\pm$ 0.062	0.023 $\pm$ 0.054

Figure 17a shows that the step length errors for all libraries deviate significantly from zero, failing to meet the accuracy requirement (mean error must be less than 0.05 m). The mean error of both the fixed and adjustable libraries are the same, while the partly adjustable library exhibits a larger mean error. However, the STD for all libraries met the precision requirement, which mandates a STD of less than 0.05 m, for this step size. In Figure 17b, similar proportions of step length errors were observed for all three libraries, with a significantly smaller STD compared to Figure 17a. Figure 17c shows comparable proportions of step length errors, with the STD for fixed and adjustable libraries being similar, and slightly smaller for the partly adjustable library. Figure 17d demonstrates that the fixed library has the mean error closest to zero, followed by the adjustable library, and then the partly adjustable library with the largest mean error. For this step size, only the fixed library meets the accuracy requirement, while all libraries meet the precision requirement.

Overall, the fixed library meets the accuracy requirement for most step sizes (three of out four), followed by the adjustable library (two out of four). The partly adjustable library performed poorly, failing to meet the accuracy requirement for any step size. However, all libraries meet the precision requirement for all step sizes. Despite these differences, no significant differences were found between the three libraries. The f-statistic was 0.98, and the p-value was 0.38 from the ANOVA performed. Those values indicate no significant differences among group means and states that the variance among group means is relatively similar to the variance within groups.

Regarding step width, Figure 17a illustrates that nearly all data points from the adjustable library fall within the target boundaries, with a very small mean error of 0.01 m. The mean errors of the fixed and partly adjustable libraries are similar but slightly larger compared to the adjustable library. Additionally, the STD is smallest for the adjustable library, followed by the fixed library. All libraries meet both the accuracy and precision requirement for this step size. In Figure 17b, the mean errors of the libraries are close to zero and relatively consistent. While the STD varies slightly between the libraries, it remains sufficient for all libraries, ensuring that both accuracy and precision requirements are met. The step width data in Figures 17c and 17d exhibit similar behavior, with errors remaining small and meeting the accuracy requirement for all libraries and step sizes. However, the STDs differ among libraries, with the fixed library having the smallest STD, followed by the adjustable library. Notably, the STD of the partly adjustable library is the largest and fails to meet the precision requirement.

Overall, all libraries meet the accuracy requirement for the step width across all step sizes, and most meet the precision requirement except for step sizes 3 and 4 with the partly adjustable library. The ANOVA performed gave a f-statistic of 1.63, and a p-value of 0.20, indicating no significant differences between the libraries.

Distribution of the different step sizes of Experiment 2

(A) SL = 350 mm & SW = 500 mm

(B) SL = 350 mm & SW = 450 mm

(C) SL = 300 mm & SW = 500 mm

(D) SL = 300 mm & SW = 450 mm
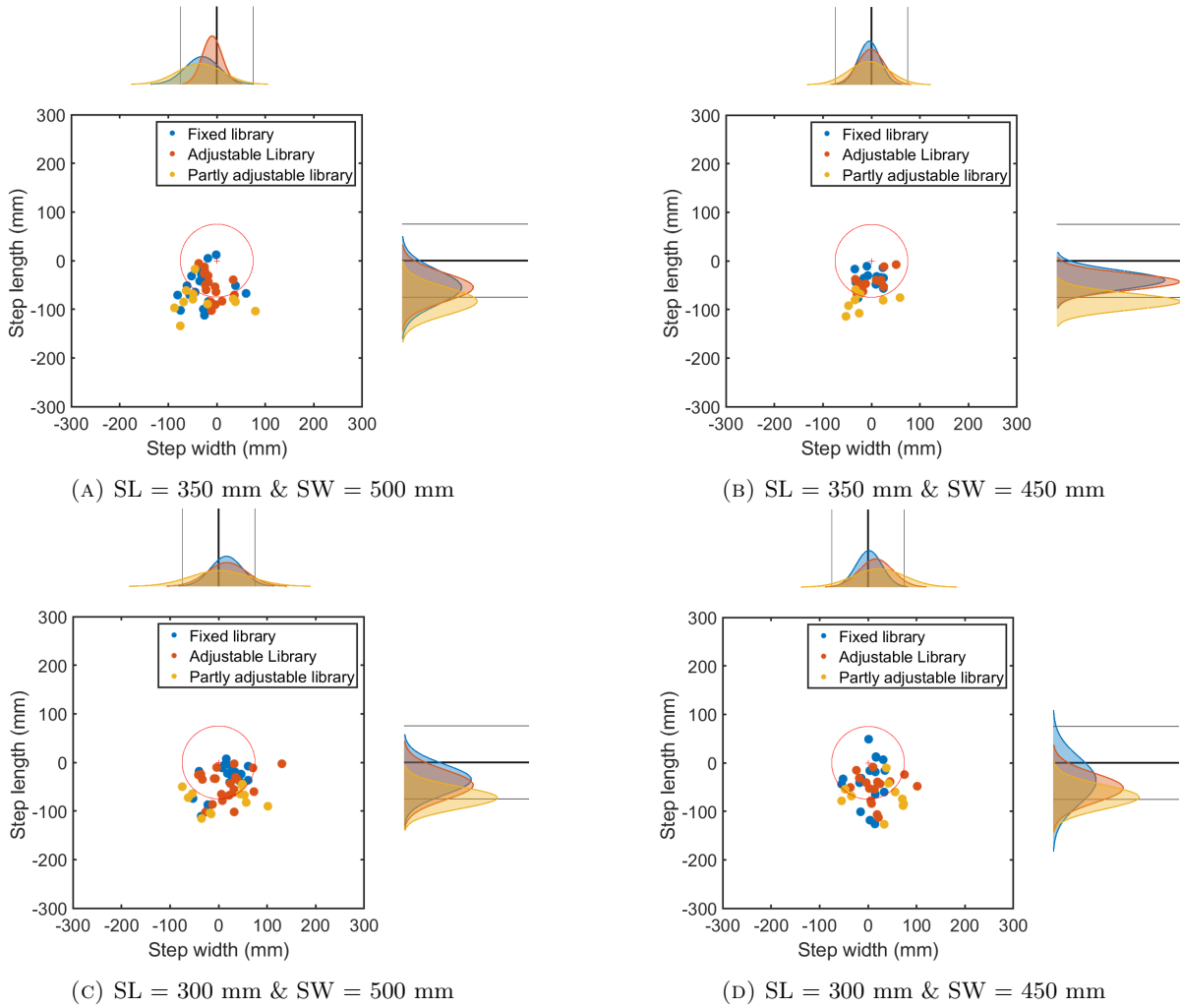
FIGURE 17: Scatter plot showing the data points and the distributions on the x- and z-axis for A) Step size 1, B) Step size 2, C) Step size 3, and D) Step size 4. The black strip indicates the point in the distribution where there is zero error, while the thin black lines show the target boundaries. The red circle highlights the area of maximum error, and the red cross indicates the position where there is no error in either step length or width.

3.2 Task load

The outcomes of the NASA-TLX are presented in Table 7. The results indicate that the mean workload is lowest for the fixed library, followed by the adjustable library. The differences in the mean workload among each library were relatively minor. The specific scores are available in Appendix 6.4.

The mean scores for the partly adjustable library exhibits the highest values, indicating a greater task load, compared to the other libraries. Particularly in terms of mental demand and frustration. The hard mental demand can be explained due to the necessity for the pilot to simultaneously adjust both heading and step size using this library. The frustration score correlates with these challenges and the pilot's fatigue. Additionally, the fixed and partly adjustable library scored higher for the physical demand compared to the adjustable library. The pilot needed to adjust the heading using these libraries, leading to notably high scores.

The longer the experiment took, the more fatigue the pilot got, leading to discomfort in the hands due to reliance on the crutches and increased leaning, especially when changing the heading himself. The pilot reported that changing the heading caused considerable discomfort in the hands. Caused by the heavy load (both horizontal and vertical forces) from both the pilot himself and the exoskeleton on the crutches. For the adjustable library, steps with the widest width, step types 1 and 3, exhibited a slight wobble, causing discomfort for the pilot. This wobble can also be seen in the output of the trajectory generator, see Appendix 6.5.

NASA-TLX comparison for the different libraries.
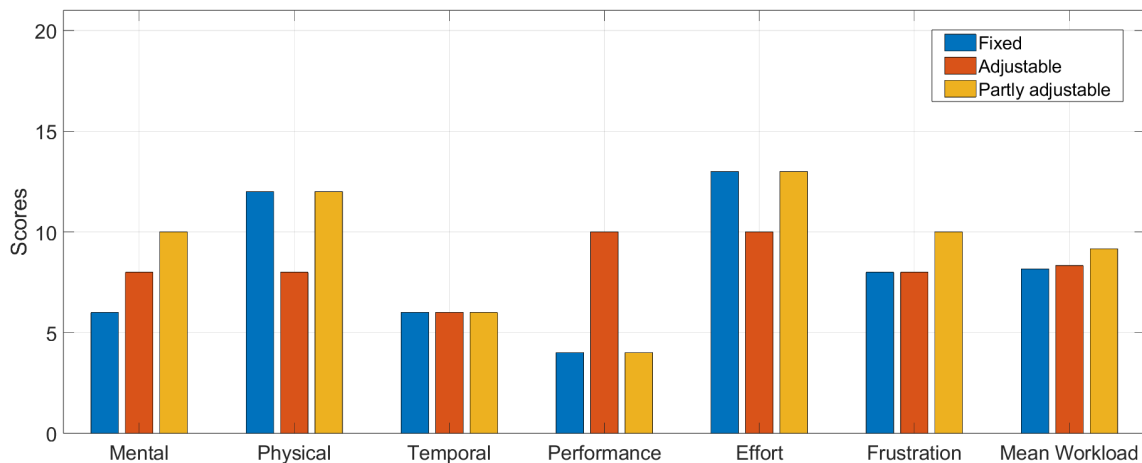
FIGURE 18: Visualisation of the outcome of the NASA-TLX for the three different libraries.

3.3 Task completion time and Transition time

The trials conducted with the fixed library were executed in the smallest task completion time, followed by the adjustable library. The task completion time was the largest for the partly adjustable library. Figure 19a shows a bar plot of the task completion times.

The libraries achieved identical rank here as for the task completion time. Figure 19b shows a bar plot of the transition times per step.

The time requirement was set to a maximum of 2 min. This criterion was met for the fixed and adjustable libraries but not for the party adjustable library. However, the transition time per step met the requirement, a maximum of 20 s, for all libraries.

Mean time and STD

(A)

(B)
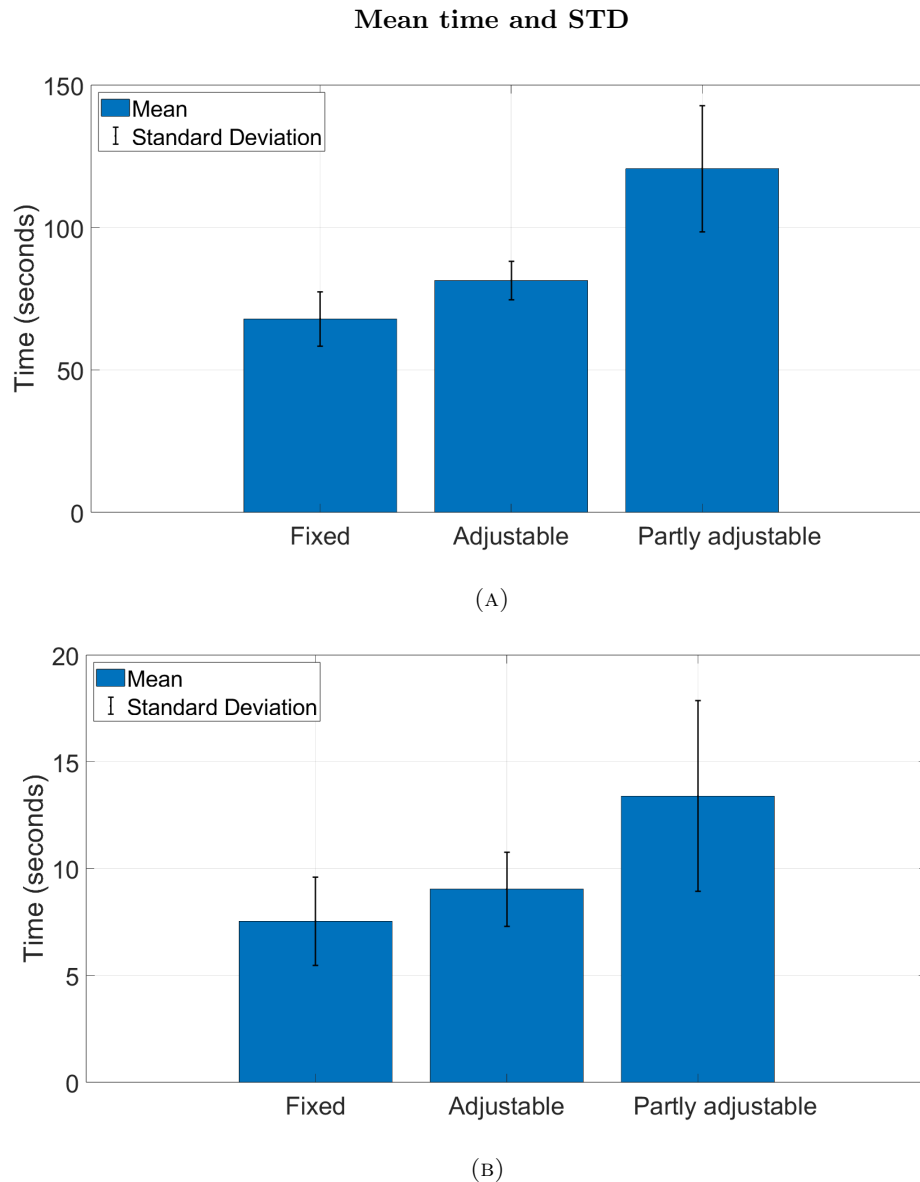
FIGURE 19: Bar graph depicting the mean time and STD (STD) per trial (a) and step (b), across the three libraries.

3.4 Joint tracking error

Figure 20 depicts the joint tracking error across all eight active joints for Experiments 1 and 2. Representing one single stance phase [4] depicting the mean error with the corresponding STD obtained from all stance phases. Those are obtained from the trajectories of the fixed library.

For Experiment 1, the mean joint tracking error for hip ab-/adduction of both leading and trailing legs is close to zero degrees, with a slightly small STD. Conversely, in Experiment 2, this mean error is larger and predominantly positive. This implies that the measured joint angles were larger than the desired joint angles when the joint angles were positive, and conversely, it signifies the opposite when the torques were negative. The STD in Experiment 2 is slightly larger compared to the STD in Experiment 1.

Regarding hip flexion/extension, the mean tracking error in Experiment 1 is relatively close to zero degrees compared to Experiment 2 for both leading and trailing legs. In Experiment 2, the mean error varies between negative and positive for both legs. A negative error indicates that the measured joint angles were smaller than the desired joint angles when the joint angles were positive, while conversely, when the torques were negative, the situation was reversed. The STD is slightly larger in Experiment 2.

For knee flexion/extension of the leading leg, the mean joint tracking error is both negative and positive and relatively close to zero for Experiment 1. For Experiment 2, the mean behaves quite stable just above zero. The STD in Experiment 1 is larger compared to Experiment 2. Regarding the trailing leg, in Experiment 1, the mean error remains consistently around 1 and 2 degrees, with a very small STD. In Experiment 2, the mean error is again positive but closer to zero degrees, with a slightly larger STD compared to Experiment 1.

Concerning ankle dorsi-/plantarflexion of the leading leg, in Experiment 1, the mean joint tracking error ranges from -2.5 to 0 degrees, with a relatively large STD. For Experiment 2, the mean ranges from 0.25 to 7.5 degrees, with a large STD. For the trailing leg in Experiment 1, the mean error is quite constant and slightly above zero degrees, with a stable STD. In Experiment 2, the mean error hovers around zero degrees, with a STD comparable to Experiment 1, with more deviations.

In general, the joint tracking error is smaller in Experiment 1 compared to Experiment 2. Large joint tracking errors can have weighty influences on the position of the end effector, which will be discussed in Section 4.

---

[4]**Single stance phase** occurs during the gait cycle when only one foot is in contact with the ground while the other foot is swinging through the air [35].

Joint tracking error

(A) Hip ab-/adduction of leading leg

(B) Hip ab-/adduction of trailing leg

(C) Hip flexion/extension of leading leg

(D) Hip flexion/extension of trailing leg

(E) Knee flexion/extension of leading leg

(F) Knee flexion/extension of trailing leg

(G) Ankle dorsi-/plantarflexion of leading leg

(H) Ankle dorsi-/plantarflexion of trailing leg

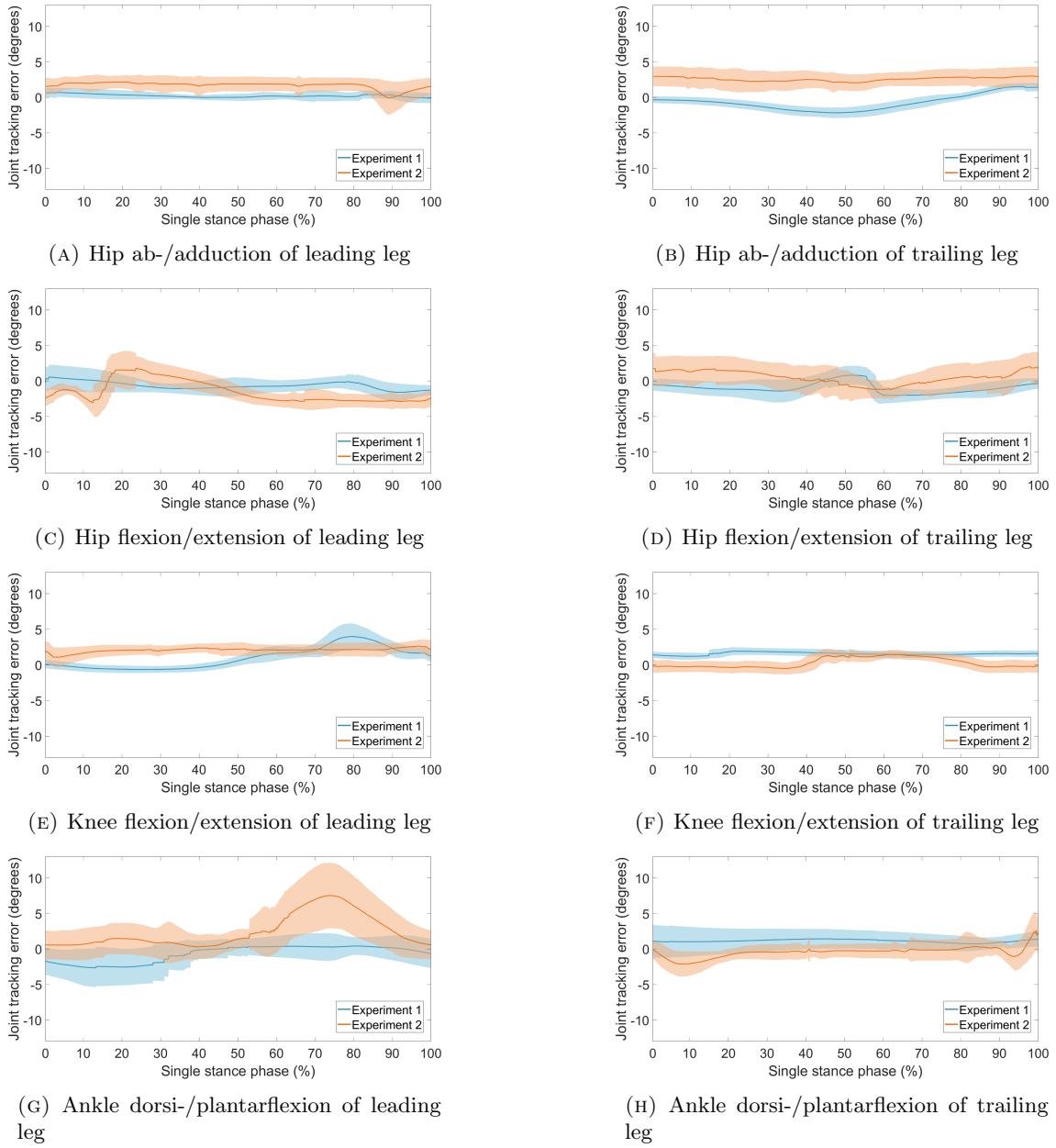FIGURE 20: Joint tracking errors of all active joints for both leading and trailing legs. The mean error of Experiment 1 is displayed in dark blue, and the STD in light blue. The mean error of Experiment 2 is displayed in dark orange, and the STD in light orange. The y-axis depicts errors in joint angles (degrees), while the x-axis represents the progression through the single stance phase (as a percentage).

3.5 Torque tracking error

Figure 21 depicts the torque tracking error across all eight active joints for Experiments 1 and 2. Representing a single stance phase depicting the mean error with the corresponding STD obtained from all stance phases. Those are obtained from the trajectories of the fixed library.

The mean torque tracking error of hip ab-adduction of the leading leg in Experiment 1 fluctuates between 0 and 2.5 degrees, with a relatively large but constant STD. In Experiment 2, the mean error exhibits significant deviations, particularly at the beginning and end of the stance phase, where the STD deviates more as well. At the start of the stance phase, the error tends to be positive. This suggests that the measured torque exceeds the desired torque when the torques are positive, and conversely, when they are negative, the situation is reversed. Conversely, towards the end of the stance phase, the mean error is predominantly negative. This implies that the measured torque falls short of the desired torque when these torques are positive, with the reverse occurring when they are negative. Concerning the trailing leg, in Experiment 1, the mean error varies considerably, ranging from -4 and 0 degrees, with a relatively large STD. In Experiment 2, the mean error fluctuates as well and lies around zero degrees with some outliers, with a slightly smaller STD compared to Experiment 1.

The mean torque tracking error of the hip flexion/extension leading leg joint in Experiment 1 starts being negative and increases slightly and ends around zero, with a relatively small STD. For Experiment 2, the mean error behaved similarly to Experiment 1 but with fewer variations, predominantly in the positive direction, and with a smaller STD. The mean error values ranged between 0 and 1 degrees. For the trailing leg in Experiment 1, the mean error remains relatively constant between 0 and 2 degrees, with a constant and relatively small STD. In Experiment 2, the mean error varies around zero degrees, with a relatively small STD as well.

The mean torque tracking error of the knee flexion/extension of the leading leg in Experiment 1 fluctuates around zero degrees with a wide range, from -5 to 4 degrees. The STD is also quite large. In Experiment 2, the mean error lies around -4 degrees and is more consistent compared to Experiment 1, with also a smaller STD. Regarding the trailing leg in Experiment 1, the mean error is very constant and lies around -2.5 degrees, with a relatively small STD. In Experiment 2, the mean error fluctuates more from -4 to 4 degrees, with a larger STD.

Regarding the leading leg in Experiment 1, the mean torque tracking error varies significantly, mostly exhibiting a negative error and including a large STD. In Experiment 2, the mean error fluctuates between 0 and 1 degrees and is very consistent, with a small STD. For the trailing leg in Experiment 1, the mean error is very constant, lying around 1 degrees. The STD is very small. In Experiment 2, the mean error fluctuates between -4 and 0 degrees, with a larger STD.

It is noteworthy that the means and STD of the torque tracking errors in Experiment 1 are in general larger and exhibit greater deviation compared to the results of Experiment 2. Further discussion on the reasoning behind this differences will be provided in the Section 4.

Torque tracking error

(A) Hip ab-/adduction of leading leg

(B) Hip ab-/adduction of trailing leg

(C) Hip flexion/extension of leading leg

(D) Hip flexion/extension of trailing leg

(E) Knee flexion/extension of leading leg

(F) Knee flexion/extension of trailing leg

(G) Ankle dorsi-/plantarflexion of leading leg

(H) Ankle dorsi-/plantarflexion of trailing leg

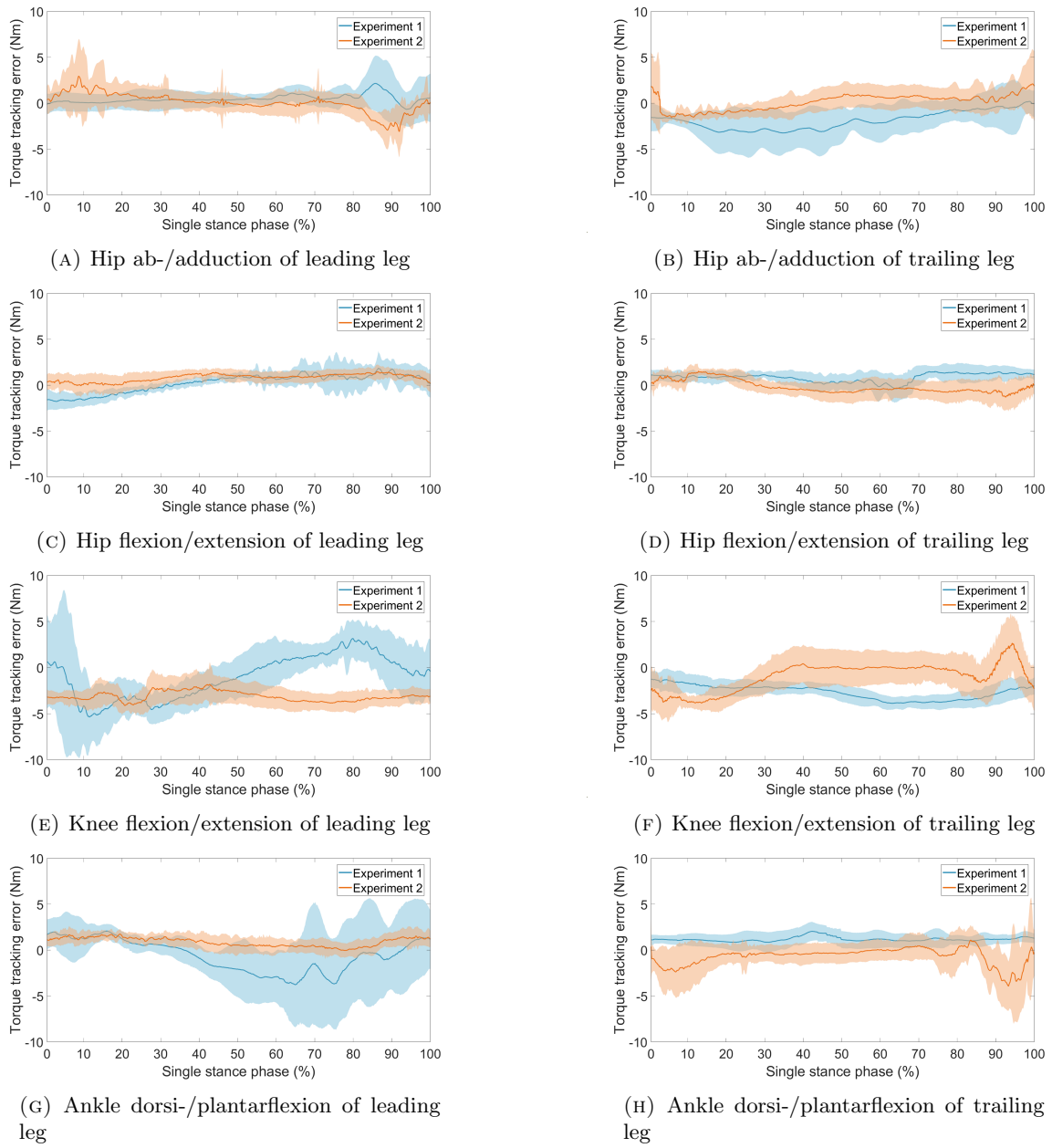FIGURE 21: Torque tracking errors of the active joints for both leading and trailing legs. The mean error of Experiment 1 is displayed in dark blue, and the STD in light blue. The mean error of Experiment 2 is displayed in dark orange, and the STD in light orange. The y-axis depicts torque tracking errors (Nm), while the x-axis represents the progression through the single stance phase (as a percentage).

3.6 Saturation error

Figure 22 illustrates the saturation error of the hip ab-/adduction joint of the leading leg in Experiment 1. Representing a single stance phase depicting the mean error with the corresponding STD obtained from all 24 stance phases. The saturation is zero for this joint, indicating that the desired torques never exceed the torque limits. This pattern holds for all other joints except for the leading leg of the knee flexion/extension. Figure 23 displays a saturation error occurring just after 80 percent of the stance phase duration. This was observed in 4 out of 24 total stance phases. This aligns to the observations illustrated in Figure 21e, where the torque tracking error exhibits a large positive error. Both desired and measured torque were negative here. This suggests that the large positive torque tracking error resulted from the desired torque having a greater magnitude than the measured torque. This occurrence is caused by the desired torque exceeding the available torque limit. The system is not able to generate the intended torque. Consequently, this discrepancy explains the notable torque tracking error and saturation observed in the findings.

In Experiment 2, the saturation error remains zero during the whole stance phase for all joints. The error behaves exactly the same as for the hip ab-/adduction joint of the leading leg in Experiment 1, Figure 22. Additionally, there were no significant deviations observed in the joint tracking errors for this experiment, indicating consistency between findings.

Saturation error hip ab-/adduction leading leg Experiment 1.

FIGURE 22: Error between the desired torque and the limited torque of the leading leg hip ab-/adduction. The mean error is displayed in dark blue, and the STD in light blue.

Saturation error knee flexion/ extension leading leg Experiment 1.
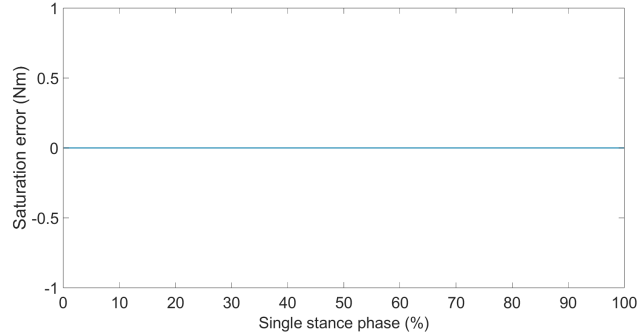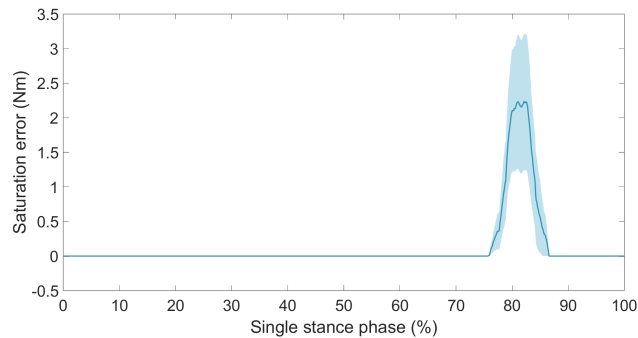

FIGURE 23: Error between the desired torque and the limited torque of the leading leg knee flexion/extension. The mean error is displayed in dark blue, and the STD in light blue.

3.7   Upper body movement

Figure 24 illustrates the roll angles of the pilot as observed in Experiment 1 and 2 for the three different libraries. Representing one gait cycle, performed with first the right leg, followed by the left leg, depicting the mean roll angles with the corresponding STDs obtained from eight gait cycles.

In Experiment 1, the roll angles for all libraries are predominantly negative in the first 50 percent of the gait cycle, corresponding to a step to the right, obtained by negative values on the z-axis. Conversely, in the second half of the gait cycle, the roll angles are mainly positive, suggesting a roll to the left. This pattern is also observed in Experiment with the (partly) adjustable libraries. In the first experiment of the partly adjustable library, the mean and STD deviate more, suggesting increased variability in lateral movement. However, the fixed library tends to exhibit positive values at the beginning and end of the gait cycle, and negative in the middle.

Roll angles of the pilot

(A) Fixed library

(B) Adjustable library

(C) Partly adjustable library

FIGURE 24: Roll angle of the pilot during both Experiments for all three libraries. The mean roll angle of Experiment 1 is displayed in dark blue, and the STD in light blue. The mean roll angle of Experiment 2 is displayed in dark orange, and the STD in light orange. The y-axis depicts the roll angles (degrees), while the x-axis represents the progression through the gait cycle (as a percentage).

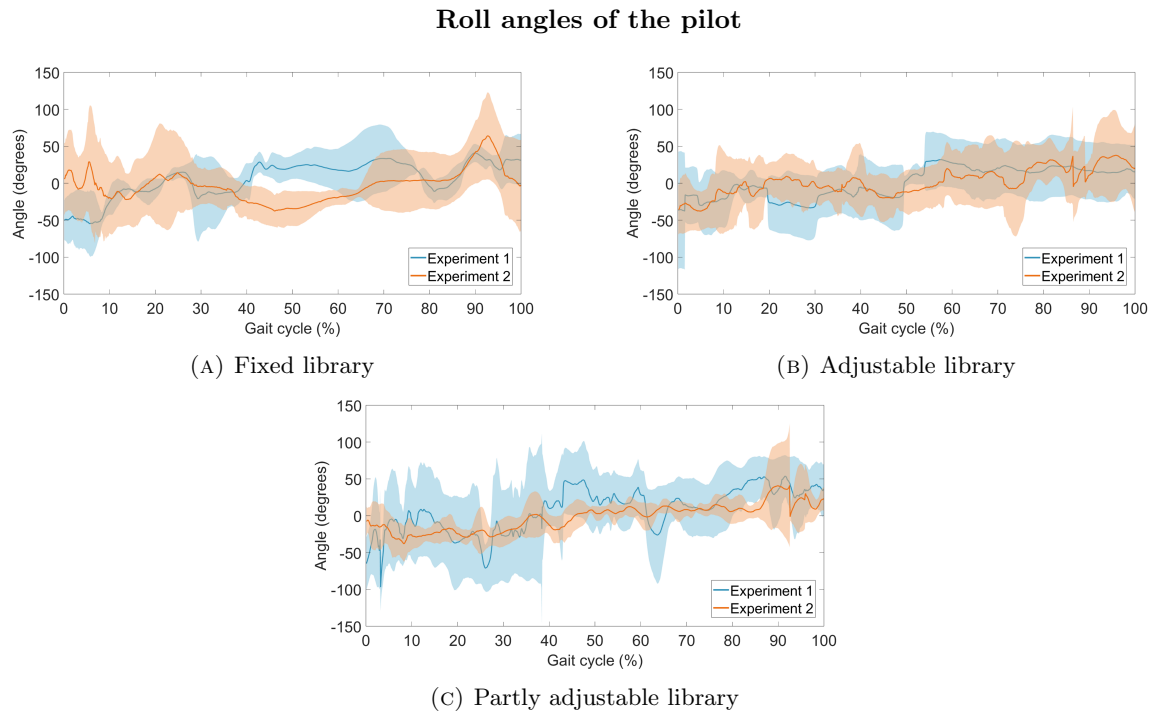Figure 25 illustrates the pitch angles observed in Experiment 1 and 2 for the three libraries. The figure represents one gait cycle, each performed first with the right leg as leading leg followed by the left one, depicting the mean pitch angle with the corresponding STD obtained from eight gait cycles.

For Experiment 1, the pitch angles remain relatively constant and just above zero degrees for all libraries. This consistent and positive angles can be attributed to the pilot's forward inclination to maintain stability while using the crutches. In contrast, Experiment 2 displays significantly larger inclinations in pitch angles. Here, the pilot had to reach targets, resulting in a greater forward lean. This increased forward lean while attempting to reach targets may be attributed to the pilot's increased focus, as well as the additional effort required to extend their arms and maintain balance during target-directed reaching movements. Furthermore, in Experiment 2, the pilot had to visually locate the targets, making it more feasible to achieve by leaning forward. The increased pitch angle is particularly noticeable in the fixed and partly adjustable libraries, where the pilot manually changed their heading.

Pitch angles of the pilot

(A) Fixed library

(B) Adjustable library

(C) Partly adjustable library

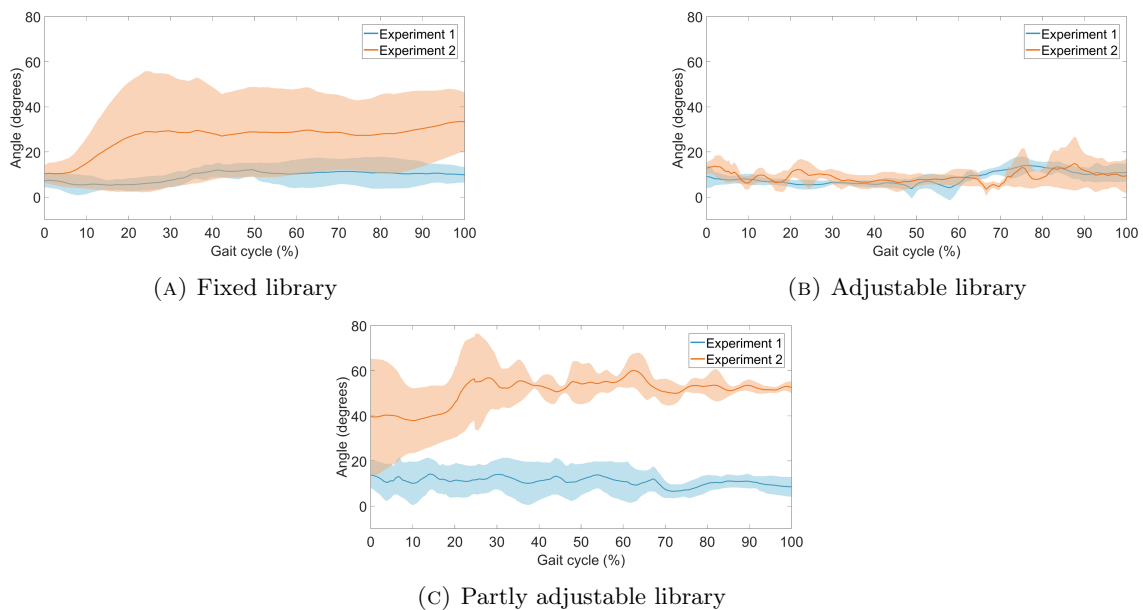FIGURE 25: Pitch angle of the pilot during both Experiments for all three libraries. The mean pitch angle of Experiment 1 is displayed in dark blue, and the STD in light blue. The mean pitch angle of Experiment 2 is displayed in dark orange, and the STD in light orange. The y-axis depicts the pitch angles (degrees), while the x-axis represents the progression through the gait cycle (as a percentage).

Figure 26 illustrates the yaw angles observed in Experiment 1 and 2 for the three libraries. The figure represents one gait cycle, each performed first with the right leg as leading leg followed by the left one, depicting the mean roll angle with the corresponding STD obtained from eight gait cycles.

In general, in the second experiment, the pilot had to actively reach for the target, which is a negative yaw angle when taking a step with the right leg and positive when taking a step with the left leg. Hence, it is logical that he rotated his body more in this scenario to achieve this. For the fixed library in Experiment 1, the mean yaw angle fluctuates around zero degrees, indicating minimal changes in heading as the pilot did not need to move to any target. However, the STD is relatively large so the heading in each trial did differ. This could also be because the pilot was unaware of where to place their feet, resulting in different forward directions being adopted during each step. In Experiment 2, the mean yaw angle during the first half of the gait cycle is negative, corresponding to a step to the right. While the mean during the second half is positive, reflecting to a step to the left.

Similar patterns are observed in the adjustable library for both experiments, with negative yaw angles in the first half and positive angles in the second half. However, Experiment 2 exhibits greater variations in both mean and STD compared to Experiment 1. This increase in variability may be attributed to the pilot's active reaching for the target, necessitating greater body rotation to achieve the goal.

In the partly adjustable library, both experiments yield divergent results compared to the other libraries. Experiment 1 shows yaw angles hovering around zero degrees with significant deviations. In Experiment 2, the mean angle starts negative and gradually increases before ending slightly positive at the end of the gait cycle. Despite expecting more extreme values and variations, the gradual change in heading observed in Experiment 2 results in less pronounced changes in yaw angles compared to the abrupt movements in Experiment 1.

Yaw angles of the pilot

(A) Fixed library

(B) Adjustable library

(C) Partly adjustable library
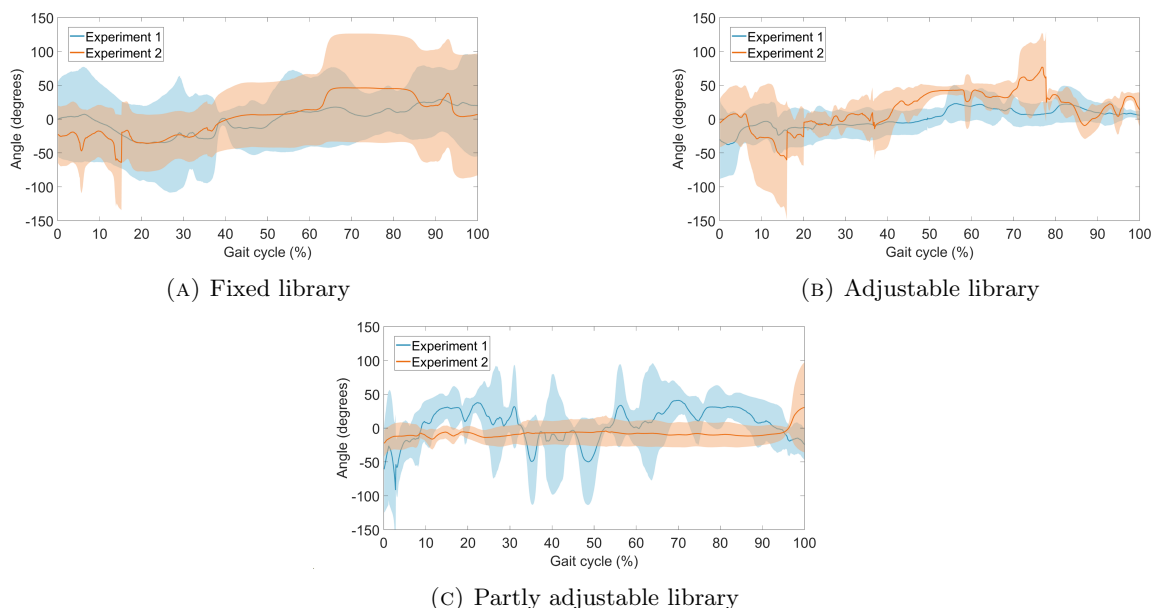
FIGURE 26: Yaw angle of the pilot during both Experiments for all three libraries. The mean yaw angle of Experiment 1 is displayed in dark blue, and the STD in light blue. The mean yaw angle of Experiment 2 is displayed in dark orange, and the STD in light orange. The y-axis depicts the yaw angles (degrees), while the x-axis represents the progression through the gait cycle (as a percentage).

4 Discussion

The aim of this study was to develop and experimentally evaluate a trajectory generator for the Symbitron exoskeleton, enabling pilots to adjust their step sizes during gait and perform movements such as the Cybathlon 2024 'Stones' task. This study constructed a trajectory generator and high-level controller including three libraries, and validated and compared those libraries.

4.1 Performance of the trajectory generators

4.1.1 Performance metrics

To assess the proximity of step lengths and widths to the desired mean and their reliability, both accuracy and precision were calculated. The accuracy requirement was defined as a maximum mean error of less than 5 cm, while precision was determined by a STD of less than 5 cm. The findings indicate that, overall, Experiment 2 outperformed Experiment 1. Experiment 2 involved the use of visual cues, specifically targets, providing the pilot with guidance on foot placement.

It was noticed that the width in Experiment 1 was not accurate in any of the cases. The pilot noted when starting with Experiment 2 that it was difficult to make the step width needed to reach the targets. However, the pilot successfully reached the targets more consistently when prioritizing reaching them. If this application will be used during the Cybathlon or even in real life, the pilot will be aware of the environment, overcoming this limitation. The pilot will be actively steering with their upper body. This will also be feasible for SCI patients, as they typically possess strong upper body muscles. Due to their inability to use their legs, they rely extensively on their upper body for daily tasks. During the first experiment it appears that the exoskeleton did not really try to force the desired step width. It could be possible that when an individual with fully mobility wears an exoskeleton designed for someone with a spinal cord injury, they may experience a noticeable difference in movement due to the weight distribution and gravitational forces acting on the device. Specifically, the legs of a person with full mobility are typically stronger and heavier than those of someone with a SCI. Consequently, the increased gravitational force exerted on the exoskeleton can impact the wearer's gait, resulting in a narrower step width compared to the intended pilot.

The step width accuracy measured in Experiment 2 was more accurate compared to the accuracy measured in Experiment 1. All widths met the accuracy requirement. For the step lengths, the results were about the same accuracy for Experiments 1 and 2, with Experiment 1 having slightly better results. In Experiment 1, the smallest step lengths (adjustable library: 0.3 m, partly adjustable library: 0.27 and 0.32 m) perform the worst. So the exoskeleton had difficulties executing such small step sizes. This was however not observed in Experiment 2. Smaller step sizes may approach the limits more closely compared to larger step lengths, potentially leading to reduced accuracy. However, this discrepancy could also be an incidental consequence.

The impedance of the exoskeleton during the experiment was not maximal. By increasing the impedance, the exoskeleton will increasingly neglect the pilot's intention. It is expected that the step lengths and widths will be more accurate when increasing the impedance due to enhanced control over joint movements. Higher impedance provide greater resistance to external forces, leading to tighter regulation of limb movement. However, the results from the joint and torque tracking errors do not directly align with these findings. This will be further discussed in Section 4.2.

The precision requirement is met for the fixed and adjustable library for all step lengths and widths in both experiments, and for the partly adjustable library in most step lengths and width. This means the results conducted in these experiments are reliable. To prepare for the actual Cybathlon, the pilot will undergo frequent training, which is likely to achieve greater consistency, and thereby a greater precision, in step lengths and widths.

Although for Experiment 2 most accuracy and precision values appear satisfactory, a closer look at the data with respect to the target boundaries and maximum error area reveals infrequent exceeding of the maximum error. Even though the accuracy and precision requirements were met in most cases, when the maximum error area is exceeded, the pilot will still miss step the target, leading to exclusion for the 'Stones' task during the Cybathlon. In Experiment 1, all libraries exceed this maximum error due to the step width.

The trajectory generator successfully generated the intended walking parameters, ensuring that the step length matches the desired value. While the step width input was the same as the actual step width by the adjustable library, it deviates by 0.02 m in both the fixed and partly adjustable libraries. Since this is a small difference, it does not fully account for the relatively large mean error observed in the experiments. These results are consistent with previous findings by Rampeltshammer et al. [11], indicating a close correspondence between the generated parameters and the specified inputs. During the experiments, it was observed that the controller effectively distinguished and selected between different step sizes. Additionally, the controller demonstrated good performance in detecting and correcting gaps in desired joint angles during the experiments as well. This suggests that the deviations probably occur by within the high-level controller.

The outcome of the ANOVA showed that the results do not significantly differ from each other, the variation between the groups is not large enough to conclude that there are meaningful differences in the variable being studied. Additionally, the consistency among the results could potentially be influenced by the sample size. When the sample size is too small, the ANOVA might not have enough statistical power to detect true differences between the groups. The sample size was 24 samples, per experiment per library. Since the current number of samples is relatively low, increasing the sample size could potentially enhance the ability to detect genuine differences between the groups more accurately.

4.1.2   Task load

The mean task load was highest for the partly adjustable library, indicating greater mental demand and frustration. The heavy mental demand likely stemmed from the pilot's need to adjust both heading and step sizes simultaneously in this library, correlating with increased frustration and pilot fatigue. Regarding physical demand and effort, the fixed and partly adjustable libraries scored higher than the adjustable library. The need for the pilot to adjust the heading manually for these libraries contributed to notably high scores. This task demands strength, focus and adds an additional challenge, making it particularly demanding for the pilot. Changing the heading demands a strong core. However, in some cases, this could be challenging, particularly for individuals with higher SCI levels, where such movements might not be feasible. This limitation represent a downside to these designs.

All trials were conducted using the fixed library, followed by trials with the adjustable library, and finally with the partly adjustable library. It was observed that as the duration of the experiment increased, the pilot experienced greater fatigue, resulting in discomfort in the hands from relying on the crutches and increased leaning, particularly when manually adjusting the heading. This fatigue and discomfort contributed to the poorer performance observed with the partly adjustable library.

The adjustable library exhibited peculiar motions for the two largest step widths (step type 1 and 3), visible in both angle trajectories and the pilot's reported experience. The smallest step size (step length is 0.27 m) for the partly adjustable library executed relatively fast, although not uncomfortable according to the pilot.

The pilot expressed dissatisfaction with the performance of the trials of Experiment 2 using the adjustable library. However, the results of the other metrics of the experiment could give a better and more objective insight in the results of the performance.

Bequette et al. investigated the task load experienced by military members wearing powered exoskeletons while navigating obstacles [36]. They reported a mean task load of 62.1 out of 100 points. Translated to a 21-point scale, this relates to approximately $62.1/100 \cdot 21 = 13.04$ points. This result appears to be worse compared to the findings of the present study (fixed library = 8.17 points, adjustable library = 8.33 and partly adjustable library = 9.17 points). However, it is important to consider that the contexts differ considerably. The powered exoskeletons used by the military likely provide more robust support, whereas the exoskeleton in the present study is designed for individuals with SCI's.

4.1.3 Time of task and transition time

The time requirement is set to a maximum of 2 min. This criterion was met for the fixed and adjustable libraries in all trials, but not for the partly adjustable library. However, the transition time per step met the requirement of a maximum of 20 s for all libraries.

The trials conducted with the fixed library demonstrated the fastest execution compared to other libraries, followed by the adjustable library. The same holds for the transition time per step. Notably, with the fixed library, the pilot did not need to change the step size, which is time consuming, particularly for less trained pilots. However, the pilot still needed to modify the heading, a task not required in the adjustable library. Changing heading appeared to take less time than altering step sizes. This discrepancy in transition time between the (partly) adjustable libraries could be explained by the pilot manually adjusting the heading in the partly adjustable library. This added additional time, and as mentioned in the task load, the pilot encountered some challenges in this aspect. The relatively large STD for the partly adjustable library could be attributed to the dual challenge of the pilot having to choose step sizes and change the heading, so adding the error caused by these challenges will add up and results in delays and thereby a greater STD.

Angles Robotics, the winner of the Cybathlon 2020, completed a task similar to the stepping stone task in just 32 s [9]. IHMC Robotics, another team utilizing a trajectory generation method based on waypoints (similar to this study), secured second place with a completion time of 34 s, with an average end effector velocity of 0.29 m/s [25]. During this study, the completion time was more than twice as long. However, it is important to note that the pilot in this study had to adjust their step sizes during the task, which naturally increased the completion time. Additionally, the pilot who operated the exoskeleton from IHMC Robotics had accumulated already 20 hours of experience with various exoskeletons over six years leading up to the Cybathlon 2016, so had even more experience 4 years later during the Cybathlon 2020 [26]. In contrast, the pilot in the current study had only walked in the exoskeleton once before, during a small experiment. Considering these factors, the performance of the libraries, especially the fixed and adjustable, in the current study can be viewed quite positively.

4.2 Tracking errors

The joint tacking errors and torque tracking errors were used to determine whether the joint angle tracking and torque regulation are sufficient.

In general, Experiment 1 exhibits smaller joint tracking errors compared to Experiment 2. While it might be expected for hip ab-/adduction joint tracking errors to be significantly larger in Experiment 1 due to larger step width errors. This is not the case; in fact, the joint tracking error for this joint is closer to zero in Experiment 1 than in Experiment 2. The discrepancy between the desired step widths and the actual step widths may stem from factors other than the desired and measured joint angles. Although joint tracking errors describes the difference between the desired and measured joint angles, other variables like mechanical constraints or external factors can impact the exoskeleton's actual movements.

Considering the joint limit ranges, the hip and knee flexion/extension have the most extensive ranges, leading to an expectation that the largest errors would occur in these joints. This is because a larger range of motion often involves more complex movements and may be more sensitive to small deviations. However, bigger errors in these joints were not consistently observed. The largest joint tracking error occurs in ankle dorsi-/plantarflexion of the leading leg, despite this joint having the smallest range. During each individual stance phase, when the desired joint angles reach a positive peak, the measured joint angles significantly surpass this value, leading to a substantial joint tracking error.

Joint tracking errors directly impact the accuracy and precision of step lengths and widths since they influence the positions of the exoskeleton's end effectors, the feet. Even minor deviations in joint angles can result in substantial differences in end effector positions. Minimizing the error between desired and measured joint angles is crucial for enhancing step length and width accuracy.

Torque tracking errors are generally larger in the leading leg compared to the trailing leg, which aligns with the larger joint angle differences and ranges observed in the leading leg. Regarding the comparison between Experiment 1 and 2, Experiment 1 tends to exhibit slightly higher overall torque tracking errors, compared to Experiment 2. The magnitude of these errors varies across the joints. It is logical that Experiment 2 exhibits a smaller torque tracking error, given that the step sizes are generally more accurate in this experiment. A smaller torque tracking error for Experiment 2 makes sense since the step sizes are in general more accurate from this Experiment. Hence, the torque regulation performed better in Experiment 2.

The saturation error remains zero for most joints. However, the knee flexion/extension joints occasionally exceed torque limits at a specific point in the gait cycle in the leading leg. This can lead to decreased reach, and thereby, inaccuracies in step sizes, as observed by the negative mean error in this library. However, inaccuracies persist even when torque limits are not exceeded, indicating additional factors influencing inaccuracies.

The joint tracking error and torque tracking errors exhibits different behaviors. The magnitude of the reference torque is influenced by the reference joint angle, as it corresponds to the amount of torque required to achieve those angles. Torque tracking errors do not necessarily correlate with joint tracking errors, as the measured torque and joint angles, which are both needed to determine the tracking errors, may differ independently from each other and are influenced by different factors, such as actuator performance and external factors. It is also uncertain whether the measured torque accurately reflects the true torque. The low-level controller is designed to make the actuators apply torque as close as possible to the desired torque. Nevertheless, due to measurement differences between torques and joint angles, factors like frictional forces on the robot (but not in the motor), such as joint friction, can influence joint angles. Furthermore, indirect torque measurements, which are known for their low accuracy [37], could introduce uncertainties into the feedback loop, affecting torque regulation.

The errors observed in the hip ab-/adduction, hip flexion/extension and knee flexion/extension joints of the controller, as reported by Meijneke et al. [12] exhibit a comparable magnitude to those identified in this study. although both studies utilize the same exoskeleton, they differ in the trajectory generator component employed. However, given that the exoskeleton and controller remain constant across both studies, it is reasonable to expect similar errors in torque and joint angle regulation, as these are determined by the high-level controller.

4.3 Upper body movement

The results obtained from the analysis of roll angles in Experiment 1 and 2 provide valuable insights into the dynamics of lateral body movement during walking with different types of libraries. The consistent pattern of predominantly negative roll angles in the first 50 percent of the gait cycle, followed by mainly positive angles in the second half, suggests a coordinated shift in weight and balance as the pilot transitions from stepping with one leg to the other. Interestingly, the fixed library demonstrates a distinct pattern of positive roll angles at the beginning and end of the gait cycle, with negative values in

the middle. This observation may reflect the influence of stimuli within the lab, such as the researcher providing step size instruction from the left side of the pilot, while the screen displaying information was located to the right of the pilot. During the experiment, the pilot needed to look at the screen. These movements could have influenced the roll angles. Based on the findings concerning the different libraries, it cannot be concluded that different libraries result in varying roll angles during the experiment.

The observed differences in pitch angles between Experiment 1 and 2 offer insights in the inclination angle of the pilot during the different experiments. In Experiment 1, a consistent forward inclination is maintained to enhance stability while using crutches. Whereas Experiment 2, involving target-reaching tasks, necessitates greater forward lean for enhanced focus and task performance. The increased pitch angles observed in Experiment 2, particularly notable in libraries requiring manual heading adjustments, highlight the influence of task complexity. Since changing the heading demands a great focus, the pilot tends to adopt a increased inclination angle.

The yaw angle variations observed in Experiment 2, where the pilot actively reaches for targets, reflect the necessity of turning the body left or right to achieve the task. Conversely, Experiment 1 in the fixed library shows less changes in heading, but with notable variability likely due to inconsistent pilot positioning. In the partly adjustable library, Experiment 1 demonstrates significant yaw angle deviations, possibly influences by the pilot's need to communicate and access information. In Experiment 2, the gradual change in heading leads to less pronounced yaw angle changes compared to the abrupt movements in Experiment 1. This observation may reflect again the influence of the researcher on the left side, and the screen on the right side of the pilot. Based on these results, it is not possible to identify a specific and consistent difference in yaw angle across any of the libraries.

4.4 Limitations of the study

The greatest limitation is the exoskeleton not being able to make the required step sizes for the Cybathlon 2024 'Stones' task. One approach to achieve those required step sizes is by making the exoskeleton's segment lengths longer, which requires recruiting a taller pilot. Increasing the limits of certain joint angles could partially solve the problem as well, but the segment length must still be extended. This adjustment involves modifications in the mechanical structure and software. Ideally, it would have been advantageous and more fair if the Cybathlon task had been adjusted to the pilot's height.

The pilot in this study is a healthy subject with the ability to walk, influencing the outcomes. Although the pilot claimed not to have used his lower body muscles consciously, muscle activity is inevitable. To evaluate the exoskeleton and trajectory generators, a future experiment should involve a SCI patient. The results of the study would also be more reliable if more than one participant would be included. However, due to time limits, both options could not be done within the scope of this study.

The amount of data in this study was limited. Increasing the number of trials would enhance the study's validity. When adding data, the results will be more reliable. It was not possible to investigate whether there are differences in performance of different step sizes depending on the previous step size. Differences could appear because each step was computed using the parameters of the previous step, so there could be a difference in performance depending on the previous step. It was not possible to investigate this due to a lack of data points. Increasing the number of trials would allow for this comparison and enhance the validity of the study.

The accuracy and precision values of the second experiment of the fixed library exceeded expectations. It is crucial to consider that these results might differ when dealing with larger differences between step sizes, especially since the current differences are the same value as the value for the maximum allowed mean error and STD. The outcome might deviate with larger differences. The current method of evaluation may not be entirely equitable, it could result in favorable outcomes in any of the step sizes. So it could explain the favorable outcomes for the fixed library in Experiment 2.

The high level controller regulates the joint angles and the amount of torques that should be exerted on each joint, which appears to be functioning incorrectly. Even the results obtained from the fixed library in Experiment 1 are unexpectedly poor. This library is the original trajectory generator without adjustments, and the outcomes do not align with the anticipated values. The trajectory generator's outcome parameters included accurate step lengths and widths. These parameters were validated by simulating them in a model and examining the resulting step lengths and widths. This discrepancy suggests that the regulation of joint angles and torques may not be sufficient to produce the expected outcomes.

A limitation in the upper body movement analysis was the necessity for the pilot to look at the GUI screen to view step sizes and other crucial information. Positioned to the right, the screen prompted the pilot to rotate their upper body in that direction. Additionally, the researcher's presence on the left side led the pilot to rotate their upper body to the left. This influenced primarily the yaw angles due to the pilot's turning, while also affecting the pitch angle, as the pilot needed to tilt their body slightly upwards to view the screen. Furthermore, the roll angle could potentially be affected as well since the entire body shift a bit looking at the screen.

4.5   Future directions

One key recommendation for future research involves adjusting the controller so it has a more accurate joint angle and torque tracking, ensuring that the desired step length and width align with the actual sizes. Enhanced hardware, such as high-quality sensors and actuators, combined with improved joint angle and torque feedback control and optimized joint limits, are among the strategies that could be employed to improve the joint angle and torque tracking. For simplification, this adjustment is suggested for the original trajectory generator, so the fixed library, with the expectation that it will likely enhance the performance of the other libraries.

Another critical addition to this study is another experiment with a SCI patient as the pilot to investigate performance in the absence of muscle activation. The significant difference between the results observed in Experiments 1 and 2 show the influence of visual input on the pilot's ability to navigate and place their feet accurately, this could be explained by the muscle activation in the lower body of the pilot. As previously mentioned, more data points would significantly improve the validity of this study. Distributing these trials across multiple days would decrease pilot's fatigue. This is already a good practice for the Cybathlon as well. When executing this experiment, the differences between the stone distances should be increased. Currently, this is not possible due to the kinematic constraints. To participate in the Cybathlon 2024, this should be adjusted and another experiment should be performed including those step lengths. In this further research, the partly adjustable library can be excluded, this library performs the worst on all criteria.

When participating the Cybathlon 2024, implementing a GUI on the crutch handle allows pilots to access essential information like step length, width, library mode etc. without relying on external screens. During the Cybathlon it is not possible to have an external screen, and moreover, it is more convenient anyway to have the GUI on one of the crutches. This would also ensure the pilot not having to look to a screen with all the needed information but just having to look at the crutch, allowing them to focus more on the task.

Within the tasks of the Cybathlon 2024 there is another tasks which includes a varying path including fixed objects, the 'boxes' task. The same approach could be used in this case, employing a step size menu as demonstrated in this study. However, for this task, varying length and height should be implemented instead of varying length and width.

Lastly, a research within the research group on integrating a depth sensor into the Symbitron exoskeleton is ongoing, this study is called 'Creating environmental awareness for the Symbitron exoskeleton using a depth camera', written by Anke Post. It would be advantageous to use this sensor to determine the distances between stones, eliminating the need for buttons in step size determination, facilitating easier exoskeleton control. A successful integration would require only some minor adjustments in the state

machine. However, the drawback of this integration would be that the exoskeleton is fully autonomous and the pilot does no longer have any say in the path their walking. A potential solution could involve combining both buttons and the depth sensor to maintain a balance between autonomy and pilot input.

4.6   Conclusion

In conclusion, the results obtained from Experiment 1 are very inaccurate. Conversely, the precision is slightly better compared to the outcomes of Experiment 2. In Experiment 2, the fixed library exhibits performance comparable to that of the adjustable library concerning step width accuracy and precision. Both libraries fulfill the requirements for step width, specifying that both the mean error and STD must be below 5 cm. Regarding step length, the results from the fixed are slightly better compared to the adjustable library, both meeting accuracy and precision requirements for some of the step sizes. The requirements for the task completion time and transition time per step, which should be less than 2 min and 20 s, respectively, are also met for those libraries. The partly adjustable library exhibits the worst performance across all metrics, further compounded by bearing the heaviest task load.

The answer to the research question 'Which of the three libraries from the trajectory generator and controller achieves the best accuracy, precision and fastest transition and task completion time when completing a downscaled version of the Cybathlon 2024 'Stones' task?', and therefore, the preferred option is the fixed library, with the adjustable library having second best performance. While the step lengths and widths do not all meet the requirements, the trajectory generator accurately outputs trajectories for all three libraries. Additionally, the currently introduced design of the high-level controller effectively selects the appropriate step sizes and integrates them well, including gap detecting and filling with polynomials, resulting in a smooth joint angle trajectory. However, it should be noted that joint angle and torque tracking, which were not the focus of this study, need improvement to ensure the correct step lengths and widths.

A good improvement would be enhancing the controller, and increasing the range of step sizes of the exoskeleton. Conducting additional experiments with SCI patients can validate the accuracy of the fixed and adjustable libraries under these conditions. This approach will contribute to advancing the technology of the Symbitron exoskeleton.

5 Acknowledgement

The author would like to express her appreciation to Ander Vallinas Prieto for the weekly meetings, feedback and help during this study. She gained a lot of valuable knowledge from him as well. Also Edwin van Asseldonk was a great help throughout several meetings, providing academic insights. Shahriar Sheikh Aboumasoudi made contributions to this study as the exoskeleton pilot, participating in all experiments. I am also grateful to Rai MacLean for her invaluable feedback. Lastly, gratitude is extended to all professors, PhDs and student participating in the Student Balance Control meetings for their feedback and useful insights.

During the preparation of this work, the author used ChatGPT in order to refine the language. After using this service, the author reviewed and edited the content as needed and takes full responsibility for the content of the work.

References

[1] M. Khorasanizadeh, M. Yousefifard, M. Eskian, Y. Lu, M. Chalangari, J. S. Harrop, S. B. Jazayeri, S. Seyedpour, B. Khodaei, M. Hosseini, *et al.*, "Neurological recovery following traumatic spinal cord injury: a systematic review and meta-analysis," *Journal of Neurosurgery: Spine*, vol. 30, no. 5, pp. 683–699, 2019.

[2] Mayo clinic, "Spinal cord injury," 2021.

[3] United Spinal Association, "Spinal cord injury facts and stats," 2022.

[4] World Health Organization, "Depressive disorder (depression)," 2023.

[5] A. Esquenazi, M. Talaty, A. Packel, and M. Saulino, "The rewalk powered exoskeleton to restore ambulatory function to individuals with thoracic-level motor-complete spinal cord injury," *American journal of physical medicine & rehabilitation*, vol. 91, no. 11, pp. 911–921, 2012.

[6] A. D. Gardner, J. Potgieter, and F. K. Noble, "A review of commercially available exoskeletons' capabilities," in *2017 24th International Conference on Mechatronics and Machine Vision in Practice (M2VIP)*, pp. 1–5, IEEE, 2017.

[7] X. Xue, X. Yang, H. Tu, W. Liu, D. Kong, Z. Fan, Z. Deng, and N. Li, "The improvement of the lower limb exoskeletons on the gait of patients with spinal cord injury: A protocol for systematic review and meta-analysis," *Medicine*, vol. 101, no. 4, 2022.

[8] R. Riener, "The cybathlon promotes the development of assistive technology for people with physical disabilities," *Journal of neuroengineering and rehabilitation*, vol. 13, no. 1, pp. 1–4, 2016.

[9] Cybathlon ETH Zürich, "Cybathlon 2024," 2022.

[10] Cybathlon ETH Zürich, "Cybathlon 2020 global edition results," 2020.

[11] W. F. Rampeltshammer, A. Q. L. Keemink, E. H. Asseldonk, and van der Kooij, "An optimal and versatile trajectory generation for lower limb exoskeletons," 2022.

[12] C. Meijneke, G. Van Oort, V. Sluiter, E. Van Asseldonk, N. Tagliamonte, F. Tamburella, I. Pisotta, M. Masciullo, M. Arquilla, M. Molinari, *et al.*, "Symbitron exoskeleton: design, control, and evaluation of a modular exoskeleton for incomplete and complete spinal cord injured individuals," *IEEE transactions on neural systems and rehabilitation engineering*, vol. 29, pp. 330–339, 2021.

[13] Cybathlon ETH Zürich, "Cybathlon 2021-2024, races and rules," 2022.

[14] K. A. Strausser, T. A. Swift, A. B. Zoss, H. Kazerooni, and B. C. Bennett, "Mobile exoskeleton for spinal cord injury: Development and testing," in *Dynamic Systems and Control Conference*, vol. 54761, pp. 419–425, 2011.

[15] A. Rodríguez-Fernández, J. Lobo-Prat, and J. M. Font-Llagunes, "Systematic review on wearable lower-limb exoskeletons for gait training in neuromuscular impairments," *Journal of neuroengineering and rehabilitation*, vol. 18, no. 1, p. 22, 2021.

[16] J. Kazemi and S. Ozgoli, "Real-time gait planner for human walking using a lower limb exoskeleton and its implementation on exoped robot," *arXiv preprint arXiv:1806.08574*, 2018.

[17] T. Vouga, R. Baud, J. Fasola, M. Bouri, and H. Bleuler, "Twiice—a lightweight lower-limb exoskeleton for complete paraplegics," in *2017 International Conference on Rehabilitation Robotics (ICORR)*, pp. 1639–1645, IEEE, 2017.

[18] S. A. Dalley, C. Hartigan, C. Kandilakis, and R. J. Farris, "Increased walking speed and speed control in exoskeleton enabled gait," in *2018 7th IEEE International Conference on Biomedical Robotics and Biomechatronics (Biorob)*, pp. 689–694, IEEE, 2018.

[19] R. Griffin, T. Cobb, T. Craig, M. Daniel, N. van Dijk, J. Gines, K. Kramer, S. Shah, O. Siebinga, J. Smith, *et al.*, "Stepping forward with exoskeletons: Team ihmc? s design and approach in the 2016 cybathlon," *IEEE Robotics & Automation Magazine*, vol. 24, no. 4, pp. 66–74, 2017.

[20] T. Yan, M. Cempini, C. M. Oddo, and N. Vitiello, "Review of assistive strategies in powered lower-limb orthoses and exoskeletons," *Robotics and Autonomous Systems*, vol. 64, p. 120 – 136, 2015. Cited by: 508.

[21] H. Ishiguro, T. Ono, M. Imai, T. Maeda, T. Kanda, and R. Nakatsu, "Robovie: an interactive humanoid robot," *Industrial robot: An international journal*, vol. 28, no. 6, pp. 498–504, 2001.

[22] O. Harib, A. Hereid, A. Agrawal, T. Gurriet, S. Finet, G. Boeris, A. Duburcq, M. E. Mungai, M. Masselin, A. D. Ames, *et al.*, "Feedback control of an exoskeleton for paraplegics: Toward robustly stable, hands-free dynamic walking," *IEEE Control Systems Magazine*, vol. 38, no. 6, pp. 61–87, 2018.

[23] J. W. Grizzle, C. Chevallereau, A. D. Ames, and R. W. Sinnet, "3d bipedal robotic walking: models, feedback control, and open problems," *IFAC Proceedings Volumes*, vol. 43, no. 14, pp. 505–532, 2010.

[24] J. Kazemi and S. Ozgoli, "Real-time walking pattern generation for a lower limb exoskeleton, implemented on the exoped robot," *Robotics and Autonomous Systems*, vol. 116, pp. 1–23, 2019.

[25] B. Peterson, M. Daniel, V. Subra Mani, B. Arnold, T. Craig, J. Gines, C. Gonzalez, W. Howell, B. Shrewsbury, M. Bellman, *et al.*, "Team ihmc at the 2020 cybathlon: a user-centered approach towards personal mobility exoskeletons," *Journal of NeuroEngineering and Rehabilitation*, vol. 19, no. 1, pp. 1–12, 2022.

[26] R. Griffin, T. Cobb, T. Craig, M. Daniel, N. Dijk, J. Gines, K. Kramer, S. Shah, O. Siebinga, J. Smith, and P. Neuhaus, "Design and approach of team ihmc in the 2016 cybathlon," 02 2017.

[27] J. Choi, K.-W. Park, J. Park, D.-H. Lee, E. Song, B. Na, S. Jeon, T. Kim, H. Choi, H. Woo, J.-H. Lee, B. Kim, D.-W. Rha, and K. Kong, "The history and future of the walkon suit: A powered exoskeleton for people with disabilities," *IEEE Industrial Electronics Magazine*, vol. 16, no. 4, p. 16 – 28, 2022. Cited by: 2.

[28] E. Sariyildiz and K. Ohnishi, "Analysis the robustness of control systems based on disturbance observer," *International Journal of Control*, vol. 86, no. 10, pp. 1733–1743, 2013.

[29] B. Koopman, E. H. van Asseldonk, and H. van der Kooij, "Speed-dependent reference joint trajectory generation for robotic gait support," *Journal of biomechanics*, vol. 47, no. 6, pp. 1447–1458, 2014.

[30] Aretech, "Zerog gait balance system," 2023.

[31] Spine-health.com, "All about c6-c7 spinal motion segment." `https://www.spine-health.com/conditions/spine-anatomy/all-about-c6-c7-spinal-motion-segment`, 2024.

[32] U. Bleimann, B. Humm, R. Loew, I. Stengel, and P. Walsh, *Proceedings of the Collaborative European Research Conference (CERC 2016) Cork.* 09 2016.

[33] MathWorks, "MATLAB: Anova1 function." MathWorks, 2023.

[34] E. Zwijgers, "Scatter distribution figure." `https://www.mathworks.com/matlabcentral/fileexchange/110850-scatter-distribution-figure`, 2024. MATLAB Central File Exchange. Retrieved November 20, 2023.

[35] A. Kharb, V. Saini, Y. Jain, and S. Dhiman, "A review of gait cycle and its parameters," *IJCEM International Journal of Computational Engineering & Management*, vol. 13, no. 01, 2011.

[36] B. Bequette, A. Norton, E. Jones, and L. Stirling, "Physical and cognitive load effects due to a powered lower-body exoskeleton," *Human factors*, vol. 62, no. 3, pp. 411–423, 2020.

[37] D. Kong, M. Hwang, D.-h. Kang, and D.-S. Kwon, "Indirect measure of joint torques of surgical instrument in robot-assisted laparoscopic surgery," in *2016 13th International Conference on Ubiquitous Robots and Ambient Intelligence (URAI)*, pp. 501–505, 2016.

6 Appendix

6.1 State machine

The original state machine is shown in Figure 27. four buttons were implemented in the crutches; the side far button, the side near button, the thumb button, and the trigger. In this version, two buttons are employed for walking. In state 100, the side far and near buttons initiate the state 101 for the opening step, and it is also used to execute state 102 of the opening step. After taking a step, the state transitions automatically to 103. While in state 103, the side far and near buttons direct the pilot back to state 101, enabling them to perform either an intermediate or closing step, respectively.
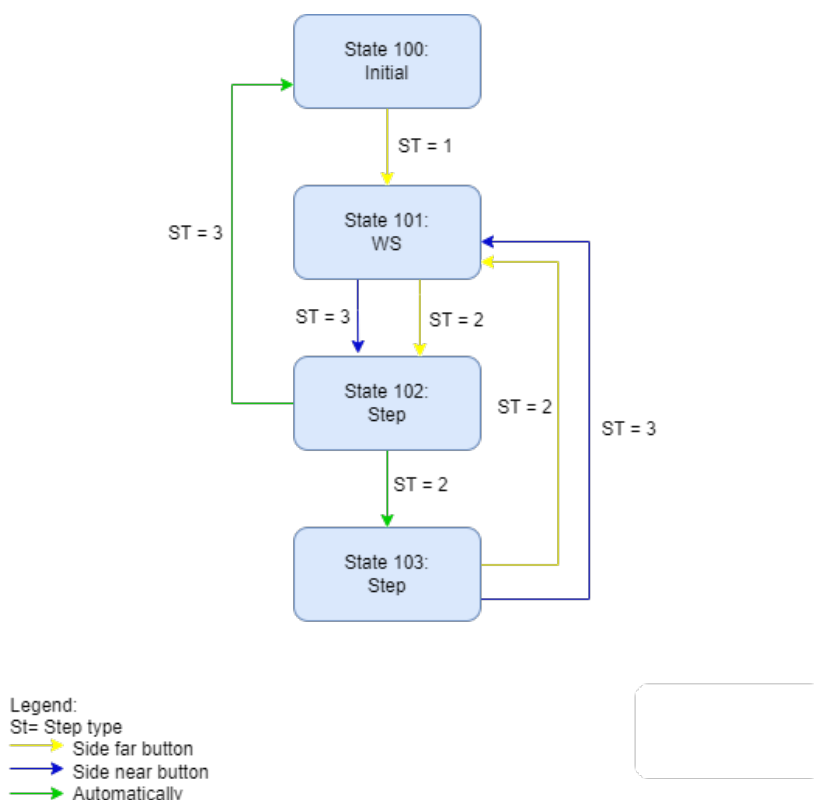

FIGURE 27: Flowchart of the state machine of the high-level controller without the adjustments.

The updated state machine, shown in Figure 28, includes two major modifications. The first adjustment was made in state 100 (parallel stance). Previously, the pilot could not choose the leg with which they would start walking, only the external operator could change this. Now, by pressing the side near button, the starting leg can be changed. This can be repeated indefinitely until the pilot transitions to another state.

The second change allows for different step sizes. When in state 100, pressing the thumb button will lead to state 200. In state 200, the step sizes can be adjusted. The side far and side near buttons are used to navigate through the step size menu, allowing the pilot to select different sized for the opening step. Similarly, in state 103, the same principle applies. When reaching from state 103 to state 200, the pilot can select different sizes for the intermediate step. When pressing the thumb button again, the state will change to the previous state (i.e. state 100 or 103). The new modifications are only accessibly for the (partly) adjustable libraries. The trigger serves to change the library, and this function remains unchanged, along with the rest of the state machine, which functions similarly to the original one.
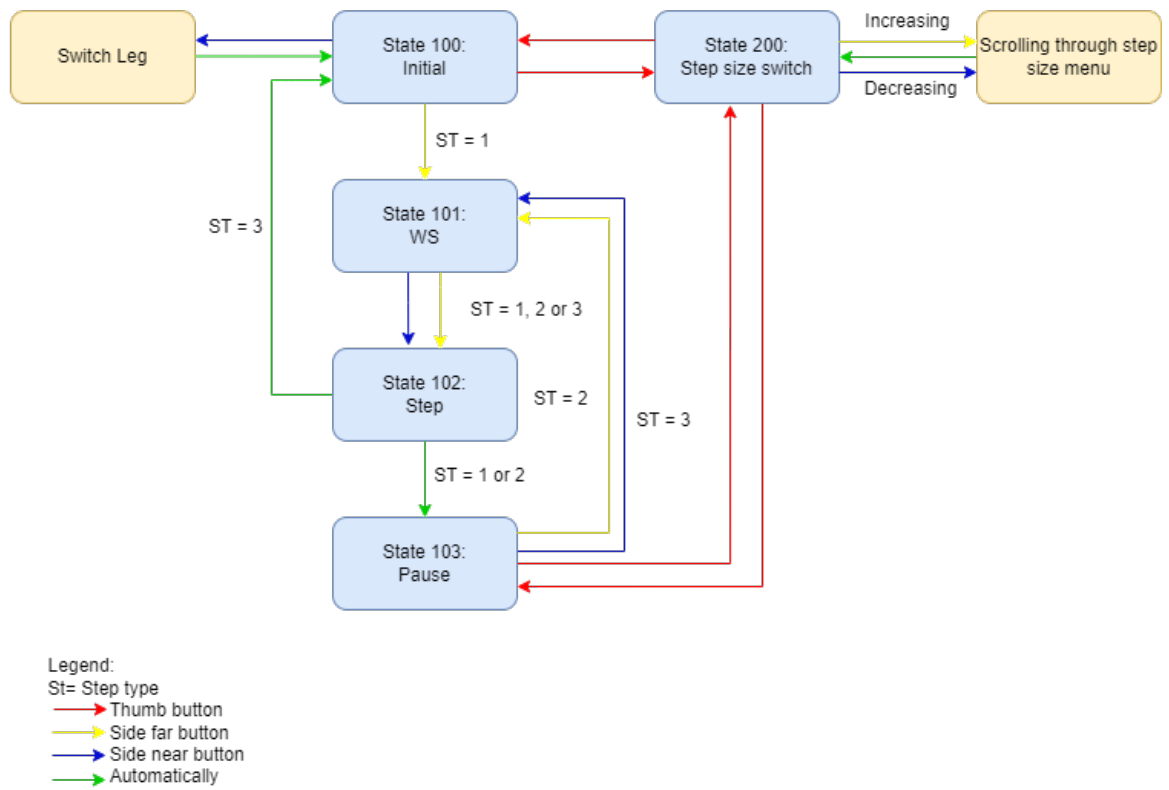
FIGURE 28: Flowchart of the state machine of the high-level controller with the proposed adjustments.

6.2 Protocol: Evaluation of Three Trajectory Generators for the Symbitron Exoskeleton

The goal of this experiment is to test which of the three proposed trajectory generators has the best accuracy, precision, and the smallest transition time when completing the Cybathlon 2024 'Stones' task. The pilot will wear the Symbitron exoskeleton in the Wearable Robotics Lab at the University of Twente which includes a marker-based motion capture (Qualisys) system. The experiment will consist of two parts, which will both be executed by a healthy subject;

In the first experiment, the subject will walk in the exoskeleton using all three proposed trajectory generators. There is no indication of the desired next step location included. The subject will also walk in the exoskeleton using all three proposed trajectory generators in the second part of the experiment. However, during this experiment, stones are placed on the ground. In this case the subject can use the stones to reach the desired step size better.

The first trajectory generator is the original path planner by Wolfgang. This generator computes steps with all the same lengths and width's. The second and third trajectory generators are modified from the original path planner. Those generators make it possible to make different step sizes within the gait. The second generator has an adjustable step length and width. The third generator has an adjustable step length and a fixed step width. In this last case the pilot has to change the heading themselves to reach the stones.

First Experiment

Description of the experiment

A healthy subject will be the pilot for this experiment. The objective of this experiment is to assess the accuracy of the trajectory generators while the visual information for proper foot placement guidance is missing. The pilot has to walk from the start to the end line while choosing the predetermined step size options. Additionally, a video of the participant executing the tasks with the assistive device will be recorded. The expected duration of the experiment:

- Help the pilot put on the exoskeleton: 10 minutes

- Preparation of experimental setup (apply the markers, setup Qualisys and apply the tape): 40 minutes

- Let the pilot play around in the exoskeleton to get used to the device: 15 minutes

- Calibration: 10 minutes

- Measurements: 3 x 20 minutes (per mode) = 60 minutes

- Resting periods: 10 minutes

- Scheduled outage: 30 minutes

- Total: approx. 170 minutes

The next data is to be collected:

1. Motion capture data of each individual trial;

2. Video recording of the participant performing the task;

3. Exoskeleton data: Joint position, velocity and torques.

Participant screening/exclusion criteria

The participant is expected to be healthy and in good physical condition. Moreover, the participant should be over 18 years old. Participants will be excluded when experiencing discomfort wearing the exoskeleton and when unexpected responses with the Symbitron exoskeleton are noticed.

Required equipment

- Symbitron Exoskeleton, including crutches

- Qualisys marker-based motion tracking system

- 29 markers

- Video camera (included in the Qualisys lab)

- Laptop with the current version of the high-level controller

- Painter's tape

Protocol

1. Measure and write down the following information of the pilot:

   - Body length;
   - Upper leg length;
   - Lower leg length;
   - Ankle-to-toe distance;
   - Heel-to-ankle distance.

2. Tape a start and end line on the ground;

3. Set the stiffness of the exoskeleton to maximum.

4. Have the participant read the user instructions of the buttons in appendix 6.1;

5. Have the participant wear the exoskeleton;

6. Place the markers on the exoskeleton and the body of the pilot on the locations given by the Qualisys model;

7. Start and calibrate the Qualisys equipment;

8. Have the operator select the Gait Selection Mode 100;

9. Start the system and the video camera;

10. Have the pilot walk steps with a fixed length and width:

    - Start in front of the start line;
    - Walk in the exoskeleton with steps of the same step lengths;
    - Stop when the end line is reached.

11. Stop the recording;

12. Repeat steps 9 to 11 three times for the step lengths defined in table 6, trial 2, and 3;

13. Have the operator switch to Gait selection mode 101;

14. Start the system and the video camera;

15. Have the pilot walk steps with varying lengths and width:

    - Start in front of the start line;
    - Make the steps defined in table 6, trial 1;
    - Stop when the end line is reached.

16. Stop the recording;

17. Repeat steps 14 to 16 three times for the step lengths defined in table 6, trial 2, and 3;

18. Have the operator switch to Gait selection mode 102;

19. Start the system and the video camera;

20. Have the pilot walk steps with varying lengths and a fixed width:

    - Start in front of the start line;
    - Make the steps defined in table 6, trial 1;
    - Stop when the end line is reached.

21. Stop the recording;

22. Repeat steps 19 to 21 three times for the step lengths defined in table 6, trial 2, and 3;

23. Turn off the Qualisys equipment;

24. Disassemble the markers from the exoskeleton and the pilot;

25. Take the exoskeleton off the pilot.

Second Experiment

Description of the experiment

The goal of this experiment is to evaluate how the trajectory generators perform when the pilot is aware where to place their feet. To verify this, the pilot is asked to walk over an unknown sequence of stepping stones. Additionally, a video of the participant executing the tasks with the assistive device will be recorded. The expected duration of the experiment:

- Help the pilot put on the exoskeleton: 15 minutes

- Preparation of experimental setup (apply the markers, setup Qualisys and apply the tape): 40 minutes

- Let the pilot play around in the exoskeleton to get used to the device: 15 minutes

- Calibration: 10 minutes

- Measurements: 3 x 20 minutes (per mode) = 60 minutes

- Resting periods: 10 minutes

- Scheduled outage: 30 minutes

- Total: approx. 175 minutes

The next data is to be collected:

1. Motion capture data of each individual trial;

2. Video recording of the participant performing the task;

3. Exoskeleton data: Joint position, velocity and torques.

Participant screening/exclusion criteria

The participant is expected to be healthy and in good physical condition. Moreover, the participant should be over 18 years old. Participants will be excluded when experiencing discomfort wearing the exoskeleton and when unexpected responses with the Symbitron exoskeleton are noticed.

Required equipment

- Symbitron Exoskeleton, including crutches

- Qualisys marker-based motion tracking system

- 29 markers

- Video camera (included in the Qualisys lab)

- Laptop with the current version of the high-level controller

- Painter's tape

Protocol

1. Measure and write down the following information of the pilot:

   - Body length;
   - Upper leg length;
   - Lower leg length;
   - Ankle-to-toe distance;
   - Heel-to-ankle distance.

2. Tape a start and end line on the ground;

3. Tape rounds on the ground for three trials, see Table 6 for the step sequences. All trials should be taped with different colors tape;

4. Have the participant read the user instructions of the buttons in appendix 6.1;

5. Have the participant wear the exoskeleton;

6. Place the markers on the exoskeleton and the body of the pilot on the locations given by the Qualisys model;

7. Start and calibrate the Qualisys equipment;

8. Have the operator select Gait Selection Mode 100;

9. Start the system and the video camera;

10. Have the pilot walk steps with a fixed length and width:

    - Start in front of the start line;
    - Walk over the stepping stones;
    - Stop when the end line is reached.

11. Stop the recording;

12. Repeat steps 9 to 11 three times for the other two trials including different stepping stone locations.

13. Have the operator switch to Gait selection mode 101;

14. Start the system and the video camera;

15. Have the pilot walk steps with varying lengths and width:

    - Start in front of the start line;
    - Walk over the stepping stones;
    - Stop when the end line is reached.

16. Stop the recording;

17. Repeat steps 14 to 16 three times for the other two trials.

18. Have the operator switch to Gait selection mode 102. Note: in this mode the pilot has to change heading himself;

19. Start the system and the video camera;

20. Have the pilot walk steps with varying lengths and a fixed width:

    - Start in front of the start line;
    - Walk over the stepping stones;
    - Stop when the end line is reached.

21. Stop the recording;

22. Repeat steps 19 to 21 three times for the other two trials.

23. Turn off the Qualisys equipment;

24. Disassemble the markers from the exoskeleton and the pilot;

25. Take the exoskeleton off the pilot.

TABLE 6: The different trials with the corresponding sequence of steps.

Trial 1	Trial 2	Trial 3
2	3	0
2 → 6	3 → 7	0 → 7
6 → 5	7 → 6	7 → 7
5 → 4	6 → 4	7 → 6
4 → 4	4 → 5	6 → 4
4 → 7	5 → 4	4 → 5
7 → 5	4 → 6	5 → 6
5 → 6	6 → 5	6 → 7
6 → 7	5 → 7	7 → 4
7 → 5	7 → 4	4 → 6
5 → 8	4 → 8	6 → 8

6.3   Normal distribution of the step lengths and widths

A histogram, qqplot, and boxplot were provided to check whether the data is normal distributed. Figure 29 shows the histogram of the output of the different libraries. The fixed library shows a clear centred bell curve, indicating a normal distribution, the adjustable library looks like a normal distribution as well, and from the boxplot of the partly adjustable library no conclusion can be drawn on the normal distribution.

FIGURE 29: Histogram of the step lengths using the fixed library (left), adjustable library (middle), and partly adjustable library (right).

Figure 30 shows the qqplot of the step length for the three libraries. The linearity of the points show that the data is a normal distribution. However, one outliers can be seen for the partly adjustable library.

FIGURE 30: qq plot of the step lengths using the fixed library (left), adjustable library (middle), and partly adjustable library (right).

Figure 31 shows the boxplot of the step lengths using the three libraries. There is just one outliers in the partly adjustable library. The box is evenly divided by the median, indication a normal distribution
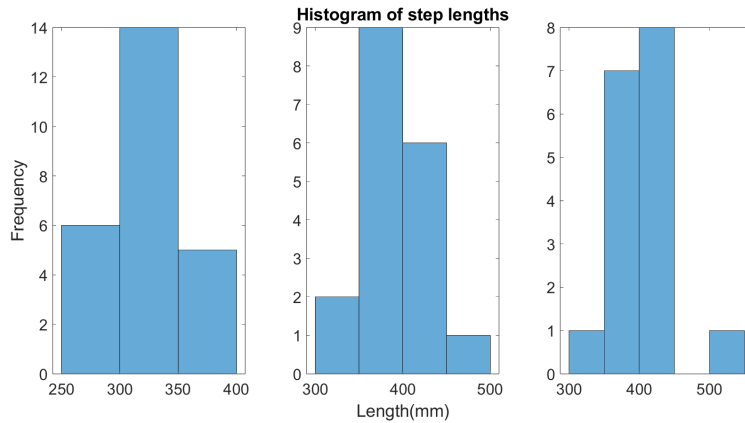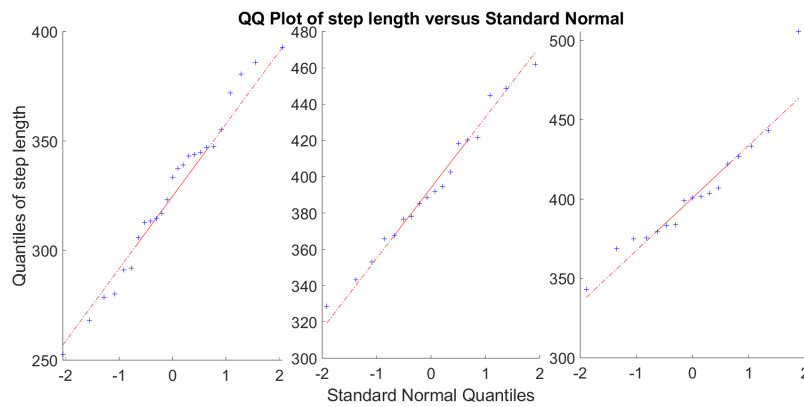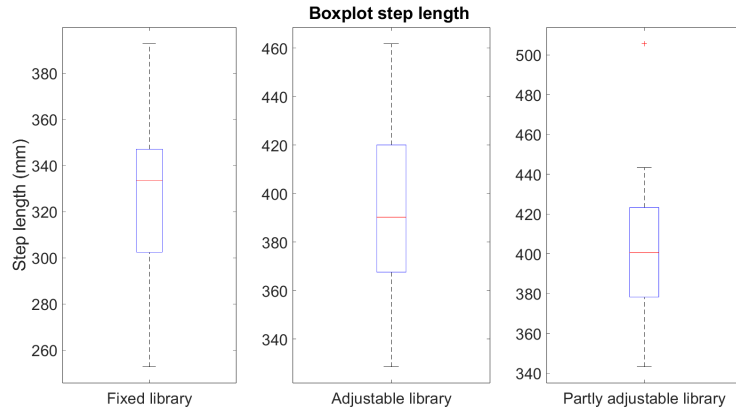
FIGURE 31: boxplot of the step length using the fixed library (left), adjustable library (middle), and partly adjustable library (right).

The same was done for the step width, which are resulted in a normal distribution.

6.4 Task load scores

TABLE 7: NASA-TLX scores for the different libraries.

	Fixed library	adjustable library	partly adjustable library
Mental demand	6	8	10
Physical demand	12	8	12
Temporal demand	6	6	6
Performance	4	10	4
Effort	13	10	13
Frustration	8	8	10
Mean	**8.17**	**8.33**	**9.17**

6.5 Output trajectory generator for the adjustable library

Figure 32 illustrates the results of the trajectory generator with a step size of 1, while Figure 33 depicts the results with a step size of 2. In the frontal plane, it is observed that the leg exhibits a wider position in the air with a step size of 1 compared to a step size of 2. Focusing on the transverse plane, it is evident that the leg undergoes a broader lateral transition in mid-air when the step size is set to 1 compared to a step size of 2.
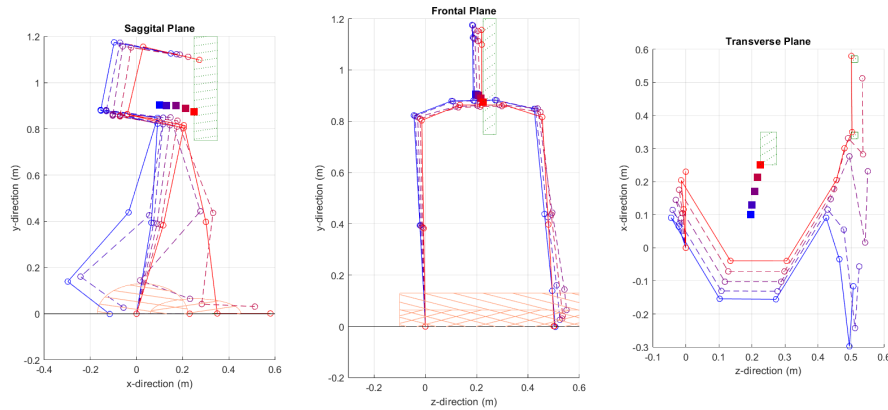
Output trajectory generator with step size 1

FIGURE 32: Output of the trajectory generator using the adjustable library, step type 1 (SL = 0.35 m, SW = 0.5 m).

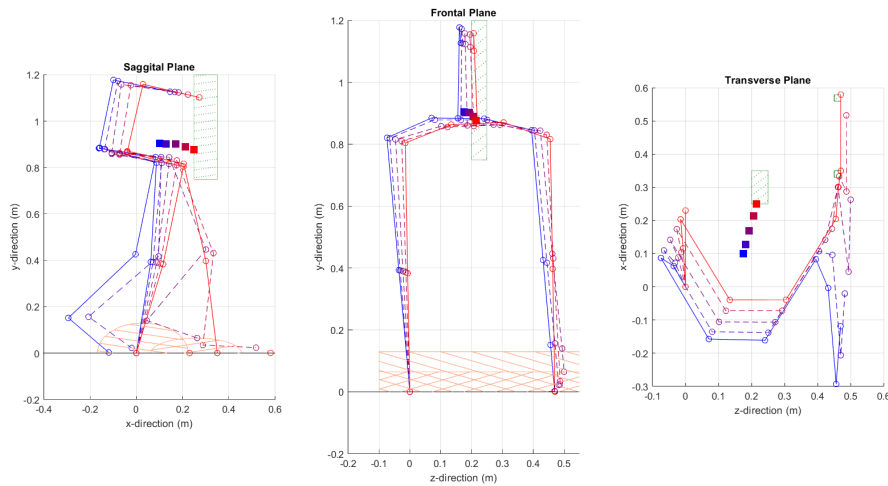**Output trajectory generator with step size 2**

FIGURE 33: Output of the trajectory generator using the adjustable library, step type 2 (SL = 0.35 m, SW = 0.45 m).

6.6 NASA-TLX

NASA Task Load Index

Hart and Staveland's NASA Task Load Index (TLX) method assesses work load on five 7-point scales. Increments of high, medium and low estimates for each point result in 21 gradations on the scales.

Name	Task	Date

Mental Demand How mentally demanding was the task?

Very Low ———————————————————————— Very High

Physical Demand How physically demanding was the task?

Very Low ———————————————————————— Very High

Temporal Demand How hurried or rushed was the pace of the task?

Very Low ———————————————————————— Very High

Performance How successful were you in accomplishing what you were asked to do?

Perfect ———————————————————————— Failure

Effort How hard did you have to work to accomplish your level of performance?

Very Low ———————————————————————— Very High

Frustration How insecure, discouraged, irritated, stressed, and annoyed wereyou?

Very Low ———————————————————————— Very High